The Astrophysical Journal Supplement Series, 166:37–68, 2006 September

SCATTER BROADENING OF SCINTILLATING AND NONSCINTILLATING AGNs. I. A MULTIFREQUENCY VLBA SURVEY

Roopesh Ojha,[1,2] Alan L. Fey,[3] T. Joseph W. Lazio,[4] David L. Jauncey,[1] James E. J. Lovell,[1] and Lucyna Kedziora-Chudczer[5]

Received 2006 February 27; accepted 2006 May 1

ABSTRACT

Multiwavelength Very Long Baseline Array observations of a sample of 49 extragalactic radio sources selected from the Micro-Arcsecond Scintillation-Induced Variability survey are presented. These observations are intended to provide a sizeable, uniform data set for the investigation of angular broadening of scintillating sources. These data will be used to compare and contrast the scattering behavior of scintillating and nonscintillating radio sources in subsequent analysis. We confirm earlier analyses that found scintillating sources to be more core-dominated than nonscintillating sources.

Subject headings: galaxies: active — galaxies: ISM — galaxies: jets — galaxies: nuclei — ISM: structure — quasars: general — radio continuum: galaxies — surveys

Online material: machine-readable tables

1. INTRODUCTION

Intraday variable (IDV) sources are compact, flat-spectrum, extragalactic sources that display intensity variations, at centimeter wavelengths, on timescales on the order of hours (e.g., Quirrenbach et al. 1992). If interpreted as intrinsic variations, these intensity fluctuations would require extremely compact, and therefore extremely high brightness temperature components within the sources. Alternatively, these variations may have an extrinsic origin and result from constructive and destructive interference of the radio wave fronts produced by refractive index variations in the ionized material along the line of sight. There is now compelling evidence that the IDV phenomenon is largely of extrinsic origin, i.e., density fluctuations in the interstellar medium induce refractive index fluctuations, which when combined with the relative motions of the scattering medium and Earth, produce intensity variations or scintillations. Time differences of up to 8 minutes have been measured in the variability pattern arrival times at widely spaced radio telescopes for the three most rapidly varying scintillators PKS 0405−385 (Jauncey et al. 2000), J1819+3845 (Dennett-Thorpe & de Bruyn 2002), and most recently PKS 1257−326 (Bignall 2003; Bignall et al. 2004, 2006). In addition, "annual cycles" in the variability characteristics have been determined for five prominent IDV sources, 0917+624 (Rickett et al. 2001; Jauncey & Macquart 2001), J1819+3845 (Dennett-Thorpe & de Bruyn 2003), PKS 1257−326 (Bignall 2003; Bignall et al. 2003), PKS 1519−273 (Jauncey et al. 2003), and B0059+3845 (Jauncey et al. 2006). Such an annual cycle arises through the changing relative velocity of the turbulent interstellar medium (ISM) and Earth in its motion around the Sun. Annual cycles are an important tool for understanding both the source structure and the behavior of the ISM (Macquart & Jauncey 2002).

In order to exhibit interstellar scintillations (ISS), a source must contain a component that is sufficiently compact (analogous to "Stars twinkle, planets don't") that its angular diameter is comparable with or smaller than the size of the first Fresnel zone of the scattering screen, i.e., on the order of tens of microarcseconds at frequencies near a few gigahertz, e.g., Walker (1998). Consistent with this requirement, Ojha et al. (2004a) have compared sources that display ISS with those that do not and find that the scintillating sources typically have smaller diameters than the nonscintillating sources. This result is particularly interesting given that these Ojha et al. (2004a) observations compared the source structure on milliarcsecond, not microarcsecond, scales.

It is not yet clear whether the absence of ISS in a source is itself an intrinsic or extrinsic effect. Extragalactic sources might be expected to have a range of intrinsic diameters, in which case only the most compact would be those that show ISS. Alternately, interstellar density fluctuations produce a rich range of observable phenomena (Rickett 1990), of which scintillations are only one manifestation. Another interstellar scattering effect is angular broadening. The magnitude of angular broadening depends on the spatial distribution and level of density fluctuations within the ionized medium. If there are multiple ionized media or an extended medium along the line of sight, then even modest amounts of angular broadening could produce apparent diameters of sources sufficiently large that the sources would not display ISS. At frequencies above the "transition frequency" (typically 3–5 GHz) in the weak scattering regime, the apparent size of an extragalactic source increases as $\lambda^{0.5}$. However, in the strong scattering regime below the transition frequency the angular size increases more rapidly, proportional to λ^2. It is in this strong scattering regime that the effects of angular broadening are expected to become accessible to ground-based VLBI.

Recently, Lazio et al. (2005) have measured low-frequency diameters of a small sample of 10 high-latitude extragalactic sources. They found that at least 70% of their observed sources had angular diameters that scale as $\theta \propto \lambda^2$, a clear indication of angular broadening through scattering. However, the amount of scattering implied by the observed angular diameters was in

[1] Australia Telescope National Facility CSIRO, P.O. Box 76, Epping, NSW 1710, Australia.
[2] NVI/United States Naval Observatory, 3450 Massachusetts Avenue NW, Washington, DC 20392-5420.
[3] United States Naval Observatory, 3450 Massachusetts Avenue NW, Washington, DC 20392-5420.
[4] Remote Sensing Division, Naval Research Lab, Code 7213, Washington, DC 20375-5351.
[5] Institute of Astronomy, School of Physics A28, University of Sydney, NSW 2006, Australia.

Report Documentation Page

Form Approved
OMB No. 0704-0188

1. REPORT DATE	2. REPORT TYPE	3. DATES COVERED
SEP 2006	**N/A**	**-**

4. TITLE AND SUBTITLE	5a. CONTRACT NUMBER
Scatter Broadening of Scintillating and Nonscintillating AGNs. I. A Multifrequency VLBA Survey	5b. GRANT NUMBER
	5c. PROGRAM ELEMENT NUMBER
6. AUTHOR(S)	5d. PROJECT NUMBER
	5e. TASK NUMBER
	5f. WORK UNIT NUMBER
7. PERFORMING ORGANIZATION NAME(S) AND ADDRESS(ES) **Library U.S. Naval Observatory 3450 Massachusetts Avenue, N.W. Washington, DC 20392-1463**	8. PERFORMING ORGANIZATION REPORT NUMBER
9. SPONSORING/MONITORING AGENCY NAME(S) AND ADDRESS(ES)	10. SPONSOR/MONITOR'S ACRONYM(S)
	11. SPONSOR/MONITOR'S REPORT NUMBER(S)

12. DISTRIBUTION/AVAILABILITY STATEMENT
Approved for public release, distribution unlimited

13. SUPPLEMENTARY NOTES

14. ABSTRACT

15. SUBJECT TERMS

16. SECURITY CLASSIFICATION OF:			17. LIMITATION OF ABSTRACT	18. NUMBER OF PAGES	19a. NAME OF RESPONSIBLE PERSON
a. REPORT	b. ABSTRACT	c. THIS PAGE			
unclassified	**unclassified**	**unclassified**	**UU**	**32**	

excess of that seen toward high-latitude pulsars. Lazio et al. (2005) considered various origins for this apparent excess scattering outside the usual ISM, namely, an extended Galactic halo and the general intergalactic medium. They concluded that if such scattering were to take place outside the ISM, then the implied scattered angular sizes at centimeter wavelengths would be so large as to prohibit ISS.

The Micro-Arcsecond Scintillation-Induced Variability (MASIV) survey (Lovell et al. 2003) was a comprehensive effort to assess the incidence of ISS in a large number of extragalactic radio sources. None of the sources common to the MASIV survey and the Lazio et al. (2005) observations exhibit ISS, consistent with the notion that the excess scattering along the line of sight has quenched the scintillations, but the Lazio et al. (2005) sample is quite small.

This paper presents observations, over a wide wavelength range, of a much larger sample of 49 extragalactic radio sources drawn from, and meeting the selection criteria of, the MASIV survey in order to compare and contrast the scattering behavior of scintillating and nonscintillating radio sources. In addition, these data supplement the structural information on scintillating and nonscintillating sources presented in Ojha et al. (2004b). Thus, these data allow further study of the milliarcsecond scale morphology of both classes of extragalactic radio sources, e.g., Ojha et al. (2004a), especially in the context of the limits on angular size imposed by the presence of ISS. A subsequent paper uses these observations to assess the impact of scattering on these sources.

2. OBSERVATIONS

Observations of 49 MASIV sources were made during three 16 hr experiments on 2003 February 17, 22, and 24 using the National Radio Astronomy Observatory (NRAO)[6] Very Long Baseline Array (VLBA). All observed sources, roughly evenly divided between scintillators and nonscintillators, were selected from the MASIV survey. The 28 scintillators are among the most highly variable sources in the MASIV sample with a minimum modulation index of 2% with some sources having a modulation index above 5%. The 21 nonscintillators were among the least variable sources with modulation index no higher than 0.2%. In order to ensure sufficient signal-to-noise at the lower frequencies, all sources had a MASIV measured mean flux density (at 4.9 GHz) of >0.3 Jy. All sources were chosen without regard to their Galactic latitude or longitude.

The observations were made at five frequencies: 0.33, 0.61, 1.6, 2.3, and 8.4 GHz. All 49 sources were observed at the lower three frequencies, but only a subset of these sources were observed at the two highest frequencies. Additional data were obtained from the United States Naval Observatory (USNO) Radio Reference Frame Image Database[7] (RRFID). This includes 2.3 and 8.4 GHz observations of sources that were not specifically observed here (with the exception of seven sources for which RRFID data were incorrectly assumed to exist). In addition, it includes images of several of these sources at 15 and 24 GHz. Any analysis of this combined data set should bear in mind that the RRFID data are not cotemporaneous with the rest of the data. A summary of all observations used in this paper is presented in Table 1. The first two columns list the sources using their J2000 and B1950 names. The third column identifies each source as a scintillator or nonscintillator, based on MASIV results. The last seven columns indicate which sources have images at the respective frequency bands. In this table the letter B is used to indicate an image from our observing program. All RRFID images are labeled with the letter R followed by a number indicating their epoch.

Observations at 0.33 and 0.61 GHz were recorded simultaneously because the 0.61 GHz signal path is limited to a 4 MHz total bandwidth in order to avoid intense radio frequency interference (RFI) at nearby frequencies. Two of the VLBA's eight IFs[8] were used to record at 0.61 MHz; the remaining six were recorded at 0.33 GHz. Dual polarization was recorded (one polarization per baseband convertor) so the total bandwidth at 0.61 GHz was 4 MHz, while at 0.33 GHz it was 12 MHz. Data were recorded using two-bit sampling to improve the sensitivity of these observations. In order to increase u-v plane coverage, we cycled through the sources, observing each source for 4 minutes per cycle. The total time on source was typically 25 minutes. At these frequencies, RFI can be a substantial problem and considerable editing of the data was necessary.

Observations at 1.6 GHz were recorded in dual polarization mode using four 4 MHz IFs and two-bit sampling yielding a total bandwidth of 16 MHz. In order to increase u-v plane coverage, we cycled through the sources, observing each source for 3 minutes per cycle. The total time on source was typically 15 minutes.

Dual polarization observations at 2.3 and 8.4 GHz were recorded simultaneously in order to optimize observing time, i.e., two 4 MHz IFs are recorded simultaneously at each frequency. However, due to a setup error in the observing schedule, only one of the 2.3 GHz IFs could be correlated. Thus, our dual polarization observations had a total bandwidth of 8 MHz at 8.4 GHz, but only 4 MHz at 2.3 GHz. Once again in order to increase u-v plane coverage, we cycled through the sources, observing each source for 3 minutes per cycle. The total time on source was typically 12 minutes.

Restoring beams were typically about 45×25 mas at 0.33 GHz, 25×12 mas at 0.61 GHz, 7×6 mas at 1.6 GHz, 5×4 mas at 2.3 GHz, and 1.5×1 mas at 8.4 GHz. Theoretical thermal noise levels in the images are approximately 1.9 mJy beam^{-1} at 0.33 GHz, 3.3 mJy beam^{-1} at 0.61 GHz, 0.3 mJy beam^{-1} at 1.6 GHz, 0.7 mJy beam^{-1} at 2.3 GHz, and 0.6 mJy beam^{-1} at 8.4 GHz. Actual noise levels are typically a factor of 2–3 worse.

Calibration of the data presented here was performed in the standard fashion within the NRAO Astronomical Image Processing System (AIPS; Greisen 1988; Bridle & Greisen 1994). The data were then exported and imaged using the Caltech Difmap imaging program (Taylor et al. 1996; Shepherd 1997). Details of the calibration and imaging of the RRFID data can be found in Fey & Charlot (2000) and references therein.

3. RESULTS

Figure 1 presents total intensity contour plots for 28 scintillating and 21 nonscintillating MASIV sources, and Table 2 lists the parameters of these total intensity images. Following the source name and frequency of observation, the next three columns list the major axis, minor axis, and position angle of the beam. The next two columns list the peak and rms flux density

[6] The National Radio Astronomy Observatory is a facility of the National Science Foundation operated under cooperative agreement by Associated Universities, Inc.

[7] See http://www.usno.navy.mil/RRFID/.

[8] In this context an "IF" (intermediate frequency) refers to a single signal path between a telescope and the correlator. Our total bandpass is divided into IFs that are adjacent in freqency. IFs should be distinguished from the narrow spectral channels into which they are subdivided as the geometrical and propagation errors affecting the data can be large enough to cause significant phase changes across an IF bandwidth.

TABLE 1
SUMMARY OF OBSERVATIONS

NAME			FREQUENCY BAND						
J2000	B1950	SCINTILLATOR	0.33 GHz	0.61 GHz	1.6 GHz	2.3 GHz	8.4 GHz	15 GHz	24 GHz
J0102+5824	0059+581	Y	nd	B	B	R9	R9	...	R11
J0217+7349	0212+735	N	nd	B	B	R1	R12	...	R12
J0343+3622	0340+362	Y	B	nd	B	...	...	...	R10
J0349+4609	...	N	B	nd	B	B	B	...	...
J0403+2600	0400+258	N	B	B	B	R2	R2	...	...
J0419+3955	0415+398	Y	B	nd	B	...	...	...	R10
J0423+4150	0420+417	N	d	nd	B	R4	R4	...	...
J0451+5935	...	Y	d	nd	B	B	B	...	...
J0502+1338	0459+135	Y	B	nd	B	...	...	...	R10
J0503+0203	0500+019	N	nd	B	B	R4	R4	...	...
J0507+4645	...	Y	B	B	B	...	...	...	...
J0509+0541	0506+056	Y	B	B	B	...	...	...	R10
J0539+1433	0536+145	N	nd	nd	B	B	B	...	...
J0607+6720	...	N	B	B	B	B	B	...	...
J0650+6001	...	N	nd	nd	B	B	B	...	...
J0654+5042	...	Y	d	nd	B	B	B	...	...
J0713+4349	0710+439	N	B	B	B	R1	R1	...	...
J0721+7120	0716+714	Y	d	nd	B	R5	R5	...	...
J0725+1425	0722+145	Y	B	nd	B	B	B	...	...
J0738+1742	0735+178	N	B	nd	B	R4	R4	R3	...
J0745+1011	0742+103	N	B	B	B	B	B	R3	...
J0757+0956	0754+100	Y	B	nd	B	R4	R12	...	R12
J0808+4950	0804+499	Y	nd	nd	B	R9	R12	...	R12
J0830+2410	0827+243	Y	B	B	B	B	B	...	...
J0831+0429	0829+046	N	B	B	B	R4	R4	...	...
J0842+1835	0839+187	N	B	nd	B	R7	R7	R3	...
J0914+0245	0912+029	Y	d	nd	B	R5	R5	...	R10
J0920+4441	0917+449	N	B	nd	B	R4	R4	...	...
J0956+2515	0953+254	N	d	B	B	R6	R12	...	R12
J0958+4725	0955+476	Y	B	nd	B	R9	R9	R3	...
J1008+0621	1005+066	Y	nd	B	B	...	...	...	R10
J1014+2301	1012+232	Y	d	d	B	B	B	...	...
J1041+5233	...	Y	B	nd	B	B	B	...	...
J1125+2610	1123+264	N	d	B	B	R4	R4	...	...
J1153+8058	1150+812	N	B	nd	B	R2	R2	...	...
J1159+2914	1156+295	Y	B	B	B	R9	R9	...	...
J1327+2210	1324+224	N	nd	nd	B	R4	R12	...	R12
J1407+2827	1404+286	N	nd	nd	B	R9	R9	...	...
J1642+6856	1642+690	Y	B	B	B	B	B	...	...
J1656+6012	...	Y	nd	nd	B	B	B	...	...
J1746+6226	1745+624	Y	nd	nd	B	R9	R9	R3	...
J1812+5603	...	Y	d	nd	B	B	B	...	...
J1823+6857	...	Y	B	nd	B	B	B	...	...
J1927+6117	...	N	nd	nd	B	B	B	...	...
J2002+4725	...	Y	nd	nd	B	B	B	...	...
J2009+7229	...	Y	B	B	B	...	...	...	...
J2022+6136	2021+614	N	B	B	B	R1	R1	...	...
J2230+6946	2229+695	Y	B	nd	B	R4	R4	...	...
J2311+4543	...	Y	nd	nd	B	B	B	...	...

NOTES.—(d) Detected but not usable; (nd) not detected; (B) Epoch 2003 February 24; (R1) Epoch 1994 July 8; (R2) Epoch 1995 April 12; (R3) Epoch 1996 April 23; (R4) Epoch 1997 January 10; (R5) Epoch 1997 January 11; (R6) Epoch 1997 December 17; (R7) Epoch 1998 August 10; (R8) Epoch 1998 December 21; (R9) Epoch 2002 January 16; (R10) Epoch 2003 May 22; (R11) Epoch 2003 September 13; (R12) Epoch 2004 February 15.

of the image. The final column indicates the contour levels used for each image.

Gaussian models were fitted to the self-calibrated total intensity *visibility data* using the Caltech Difmap package. The results of the model fitting are listed in Table 3. After the source name the following items are listed: observation frequency, component number; total component flux; distance of component from core; orientation of component with respect to the core component; length of major axis of component; axial ratio of component (1 for circular component); and orientation of major axis of component.

Ojha et al. (2004a) found a highly significant difference in the core dominance of scintillating and nonscintillating sources. In order to test whether this difference holds for the sources in our sample, following the analysis of Ojha et al. (2004a), we estimate the core dominance of the sources by calculating a "core

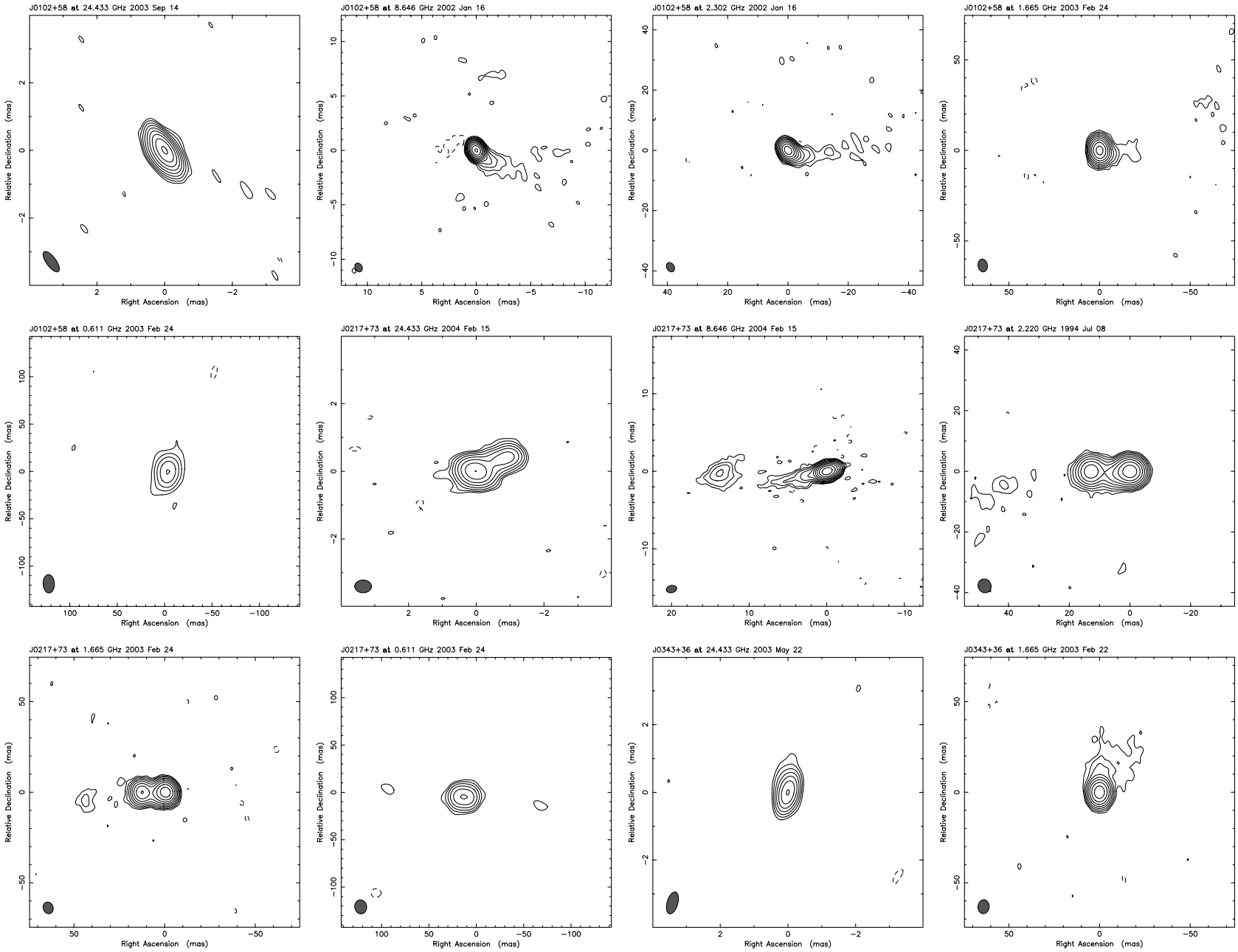

FIG. 1.—Contour plots of 49 extragalactic radio sources from the MASIV survey at radio frequencies ranging from 0.33 to 24 GHz. Table 2 lists the image parameters, and Table 3 lists the results of fitting Gaussian models to the visibility data used to generate these images. The scale of each image is in milliarcseconds. The FWHM Gaussian restoring beam applied to the images is shown as a hatched ellipse in the lower left of each panel.

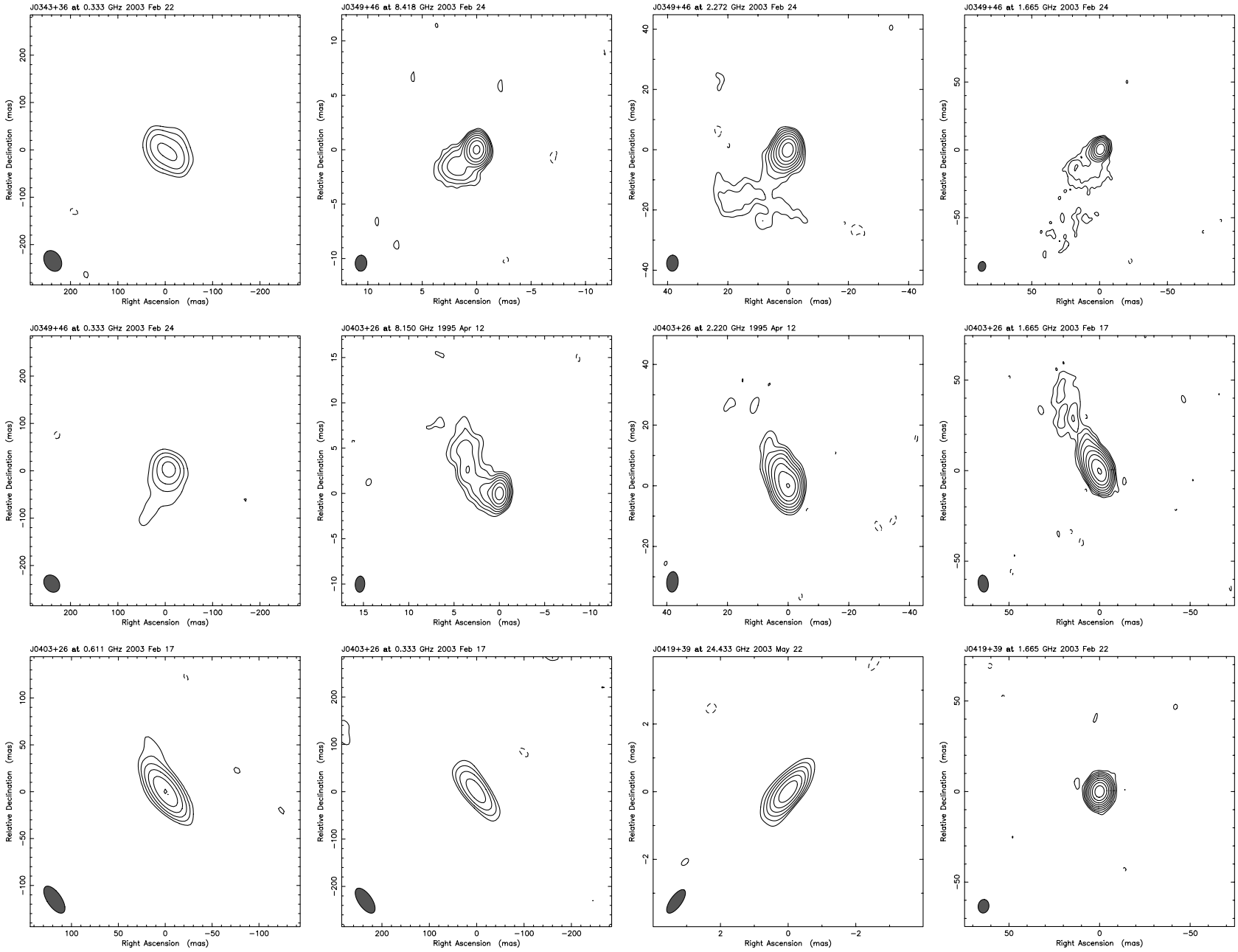

FIG. 1.—*Continued*

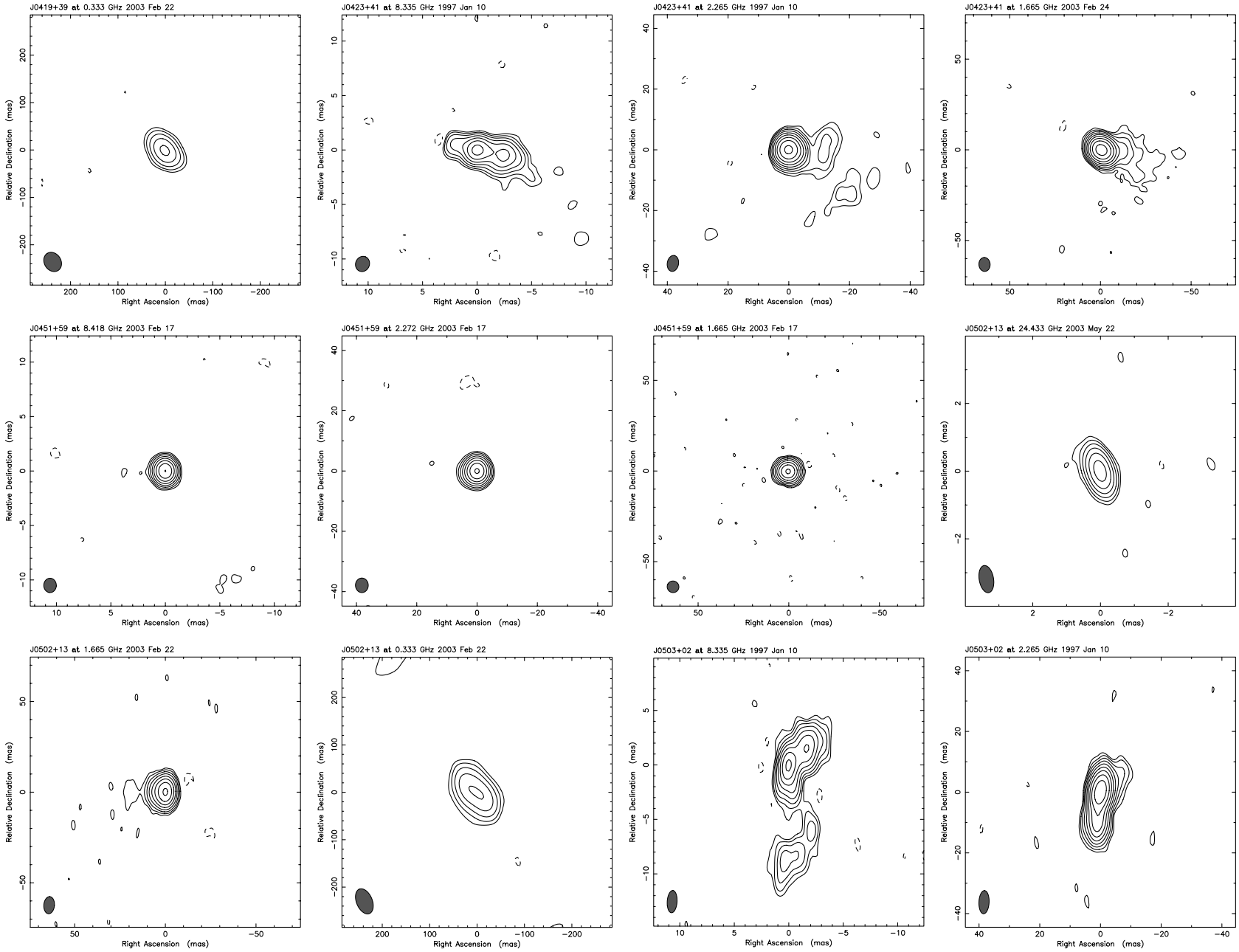

FIG. 1.—*Continued*

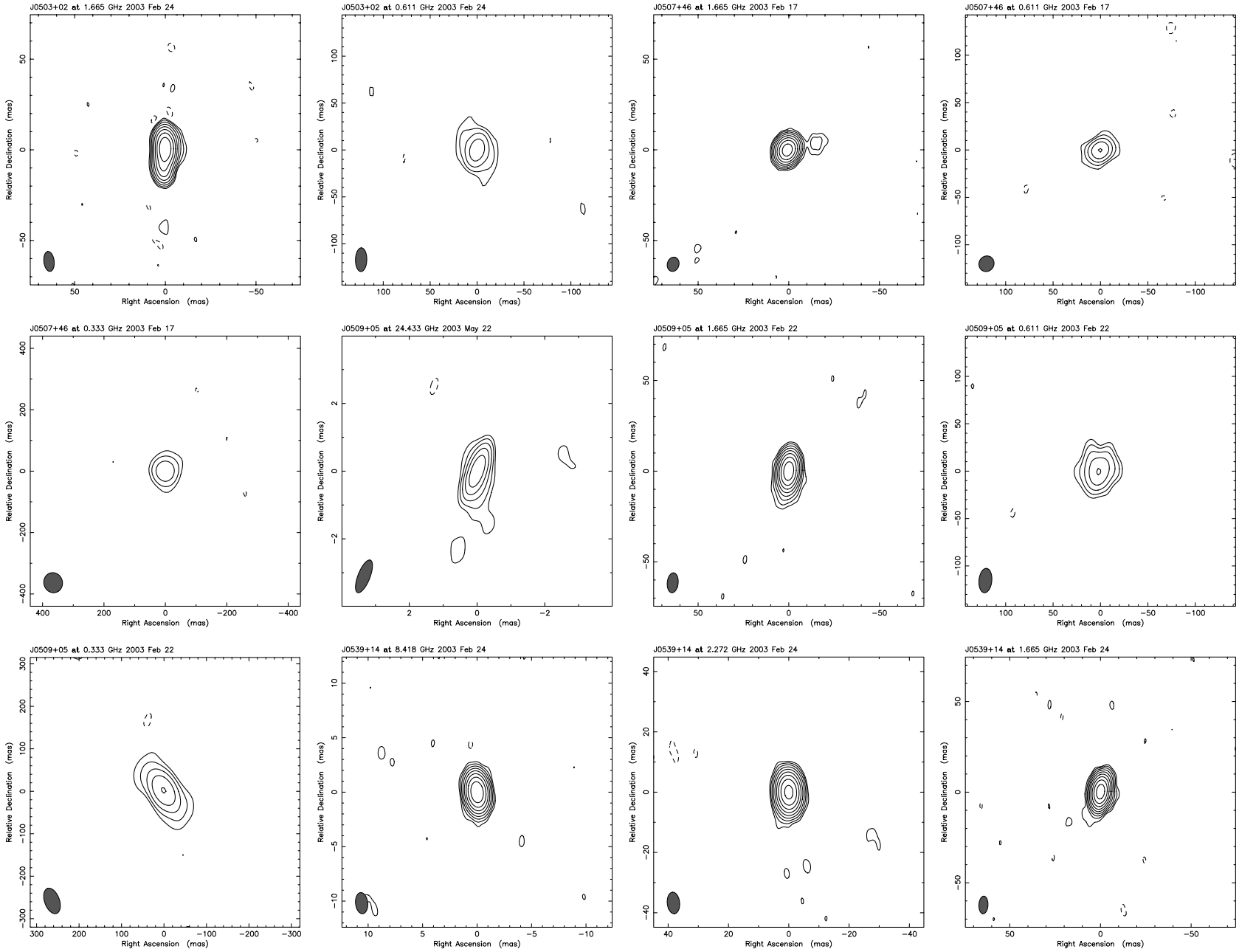

FIG. 1.—*Continued*

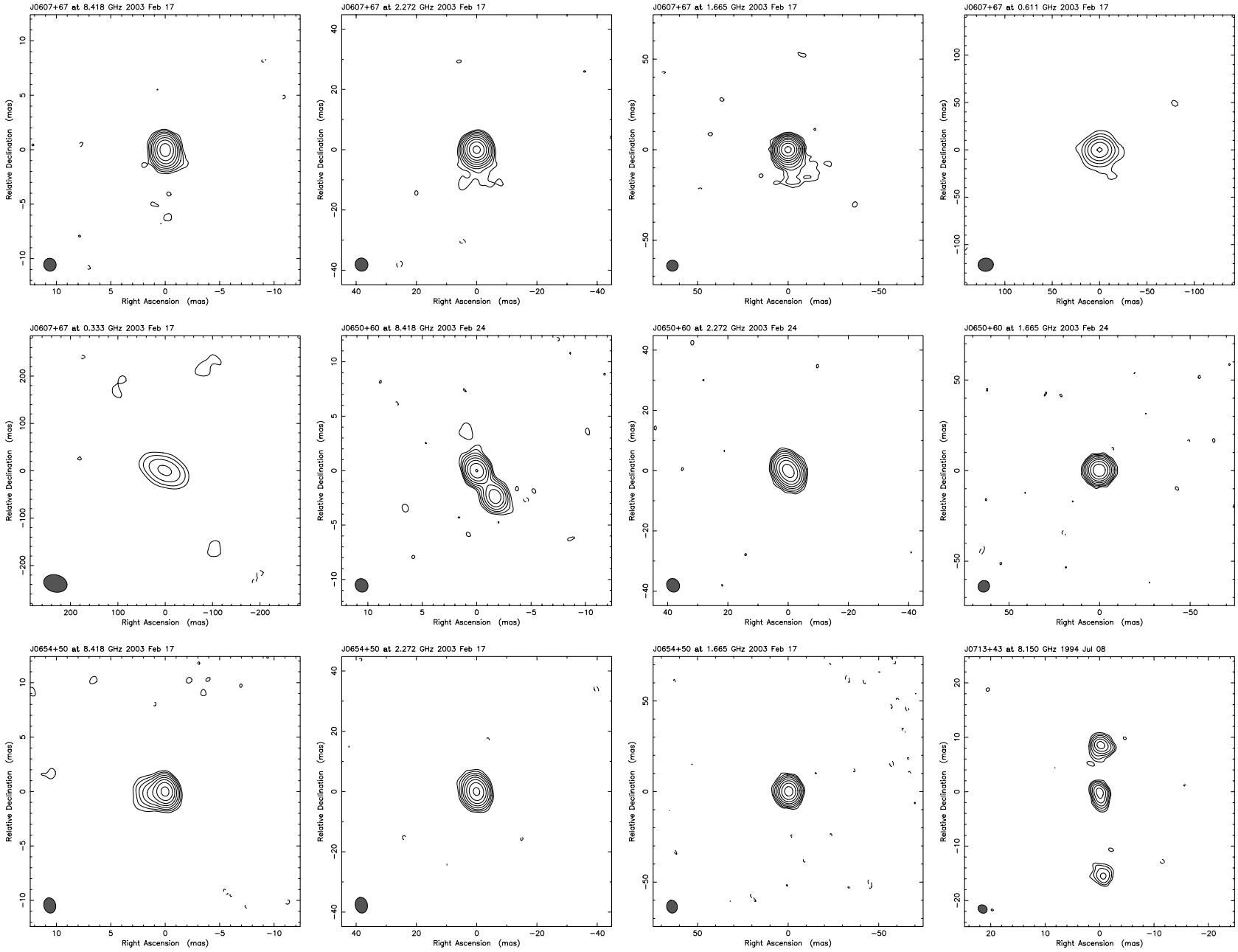

FIG. 1.—*Continued*

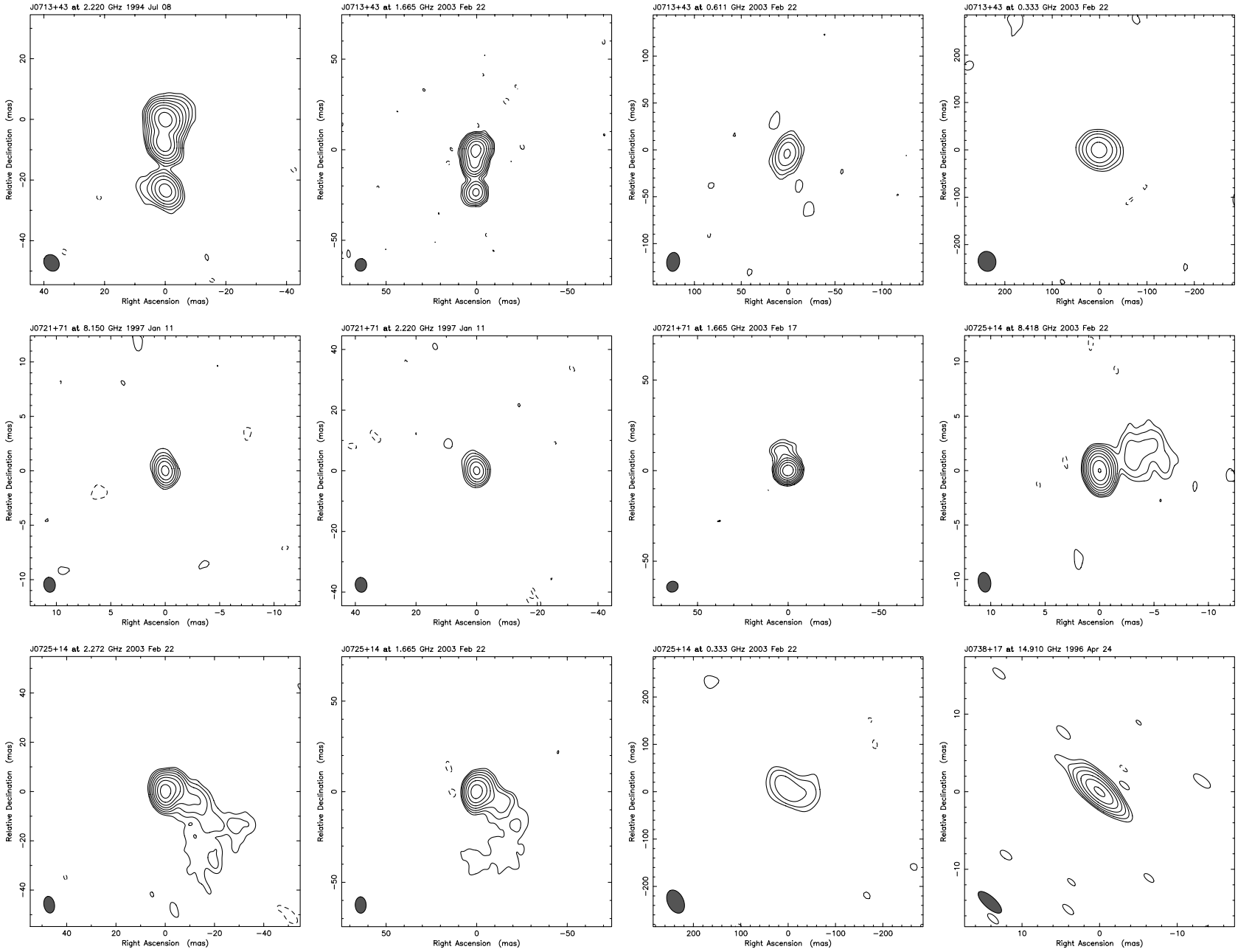

FIG. 1.—*Continued*

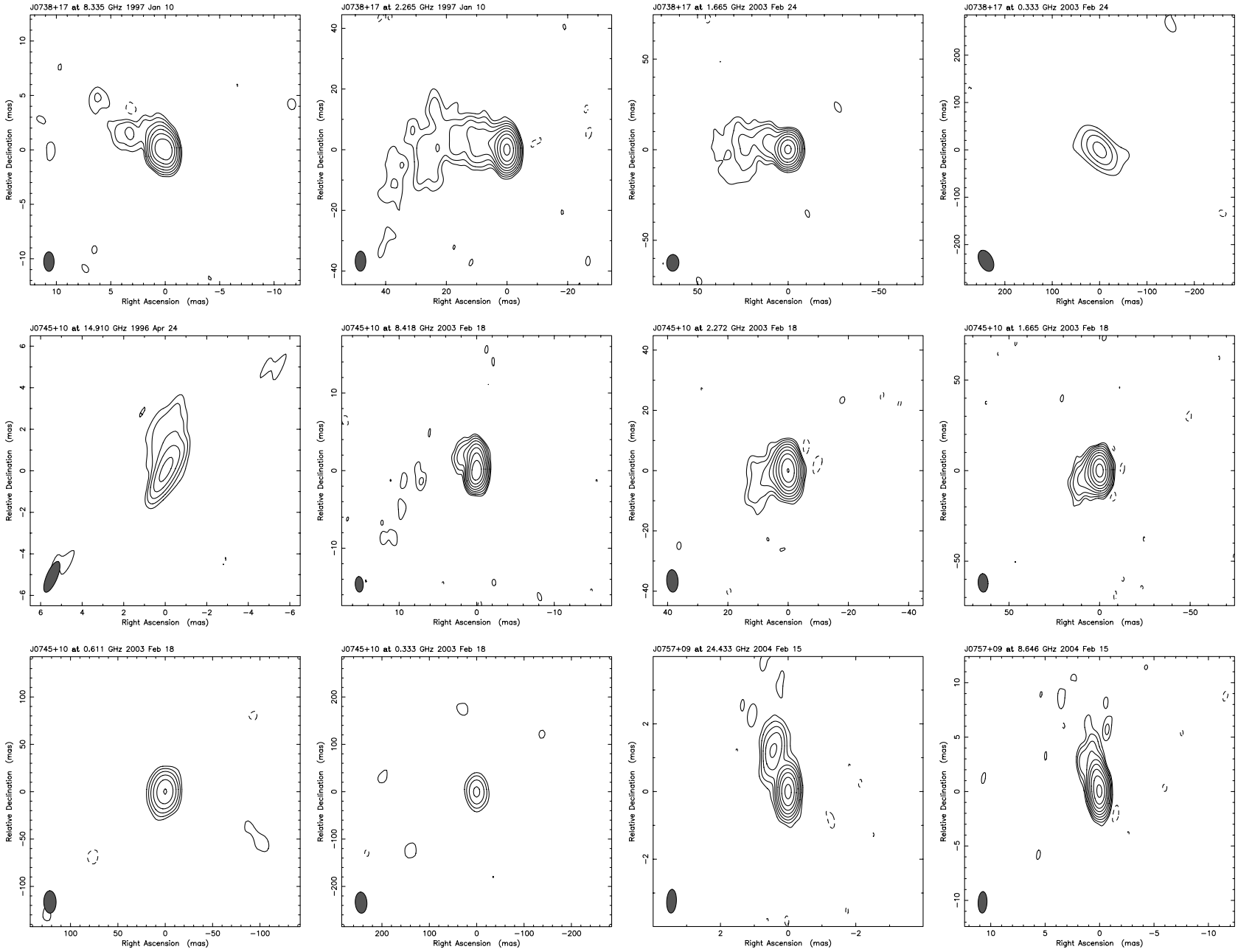

FIG. 1.—*Continued*

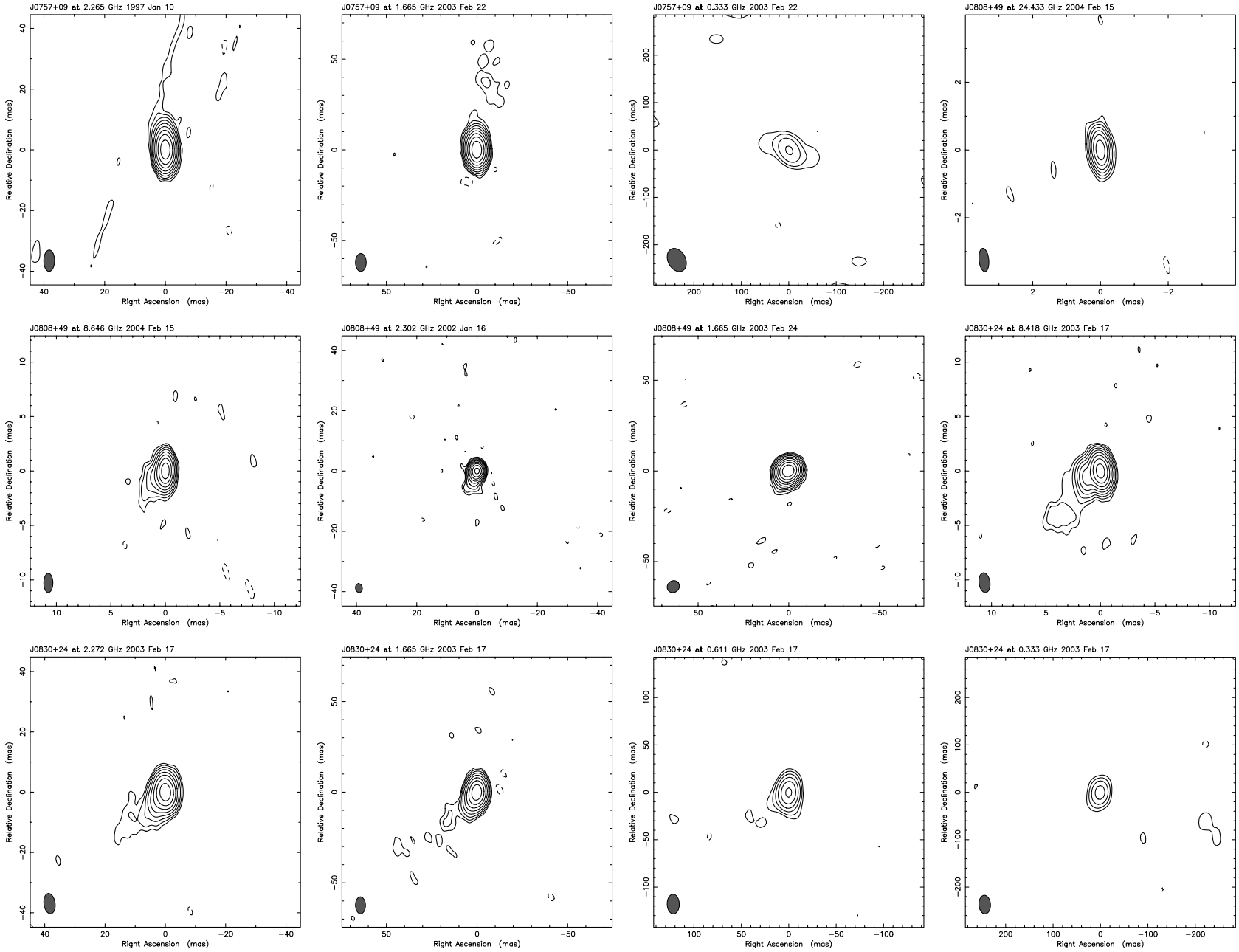

FIG. 1.—*Continued*

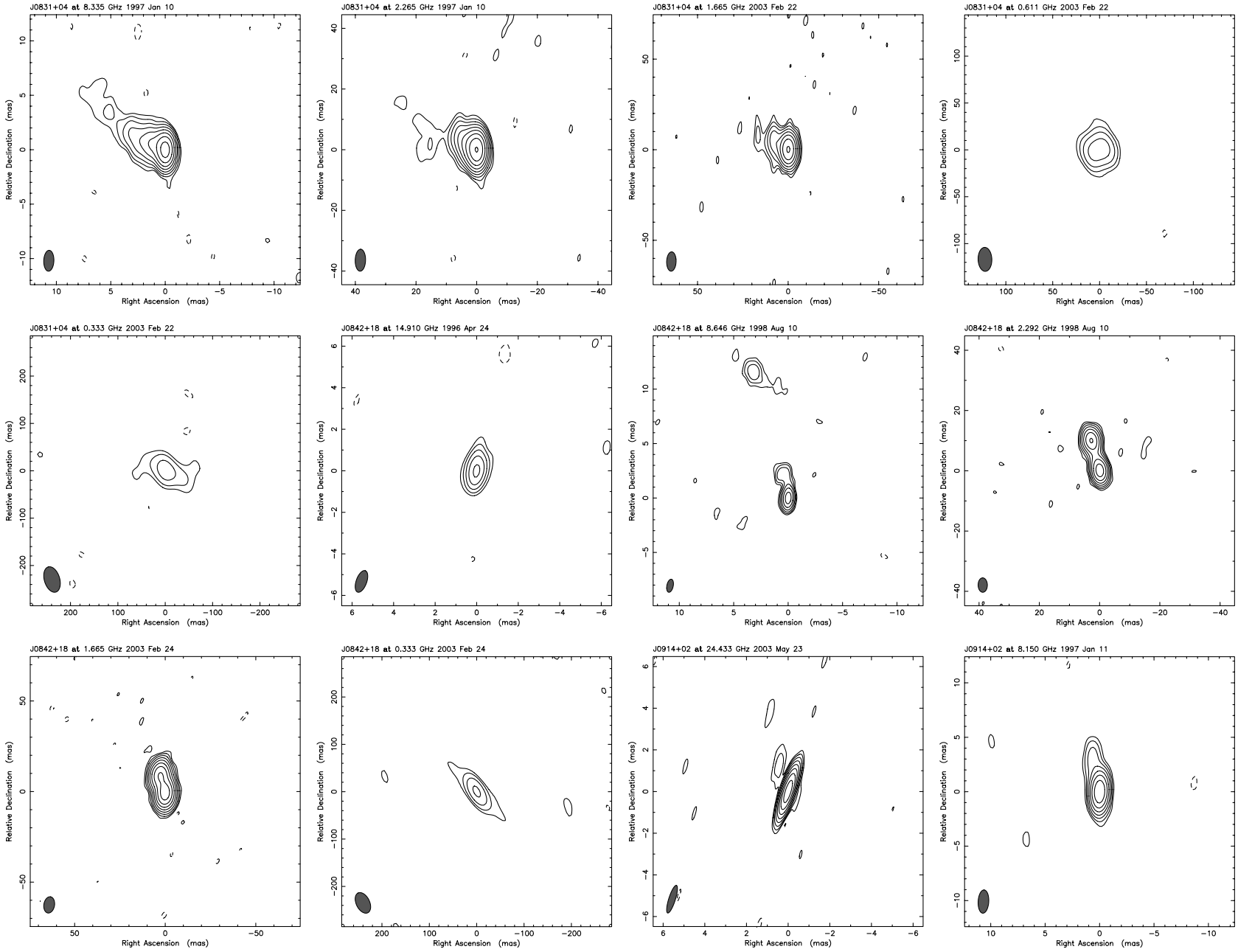

FIG. 1.—*Continued*

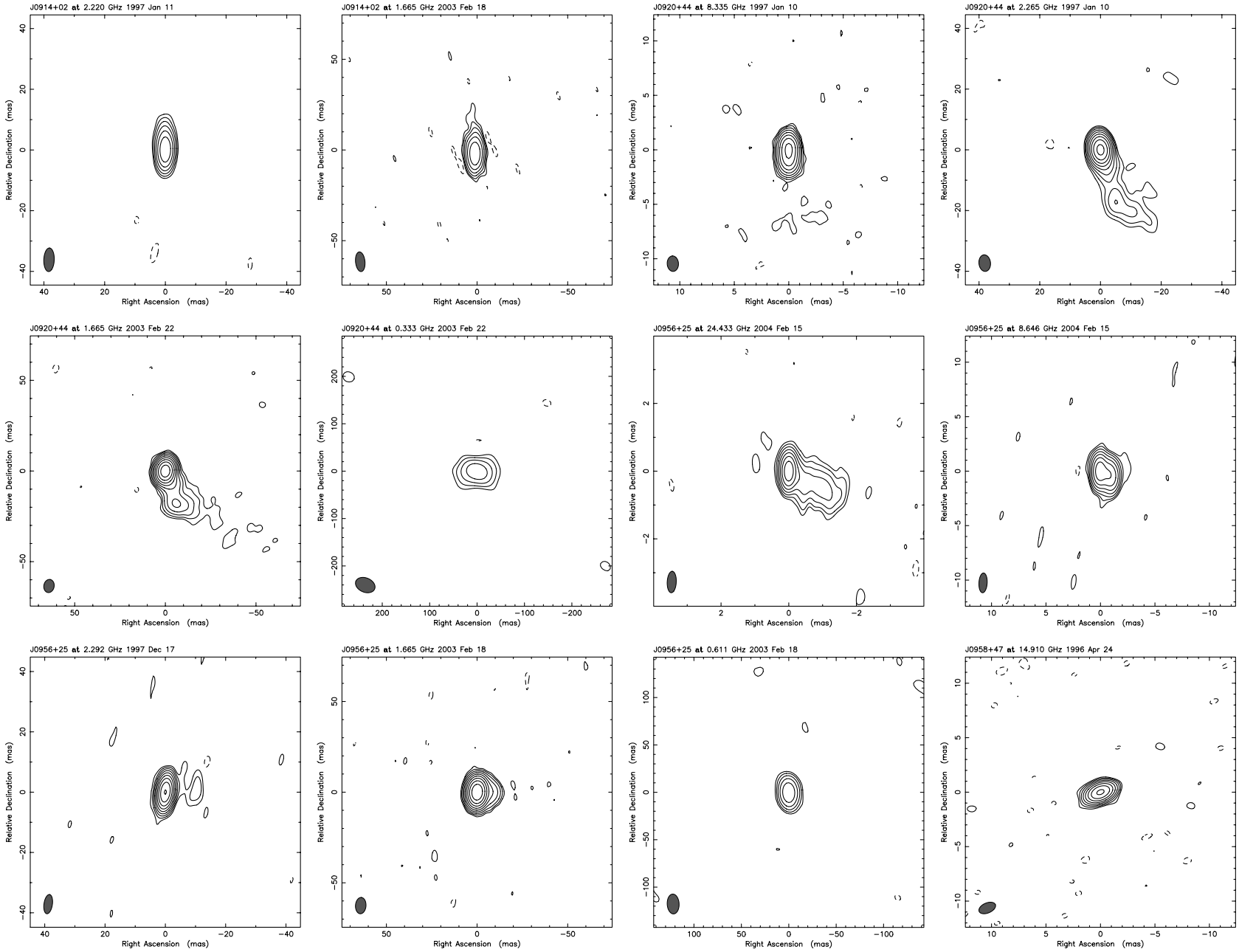

FIG. 1.—*Continued*

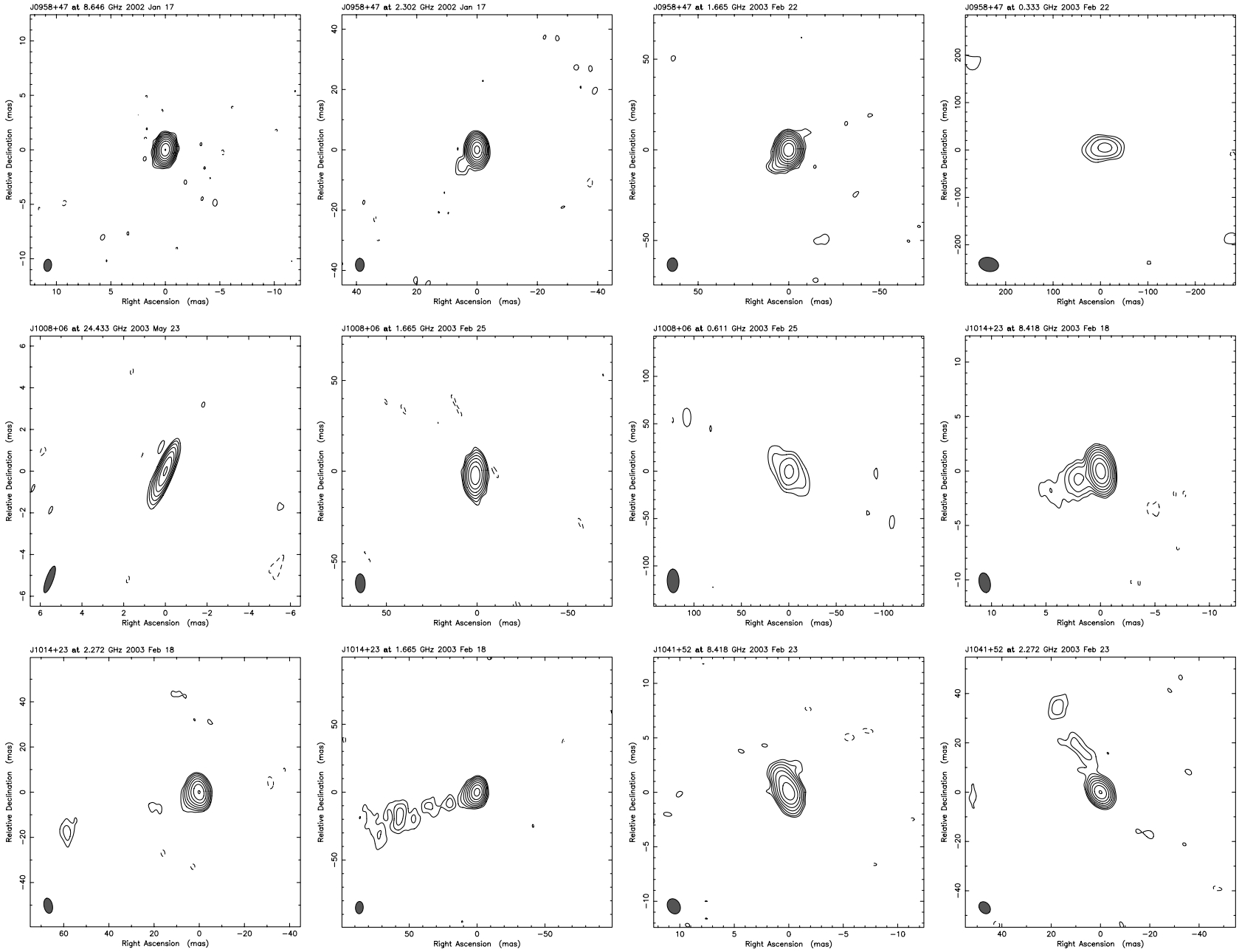

FIG. 1.—*Continued*

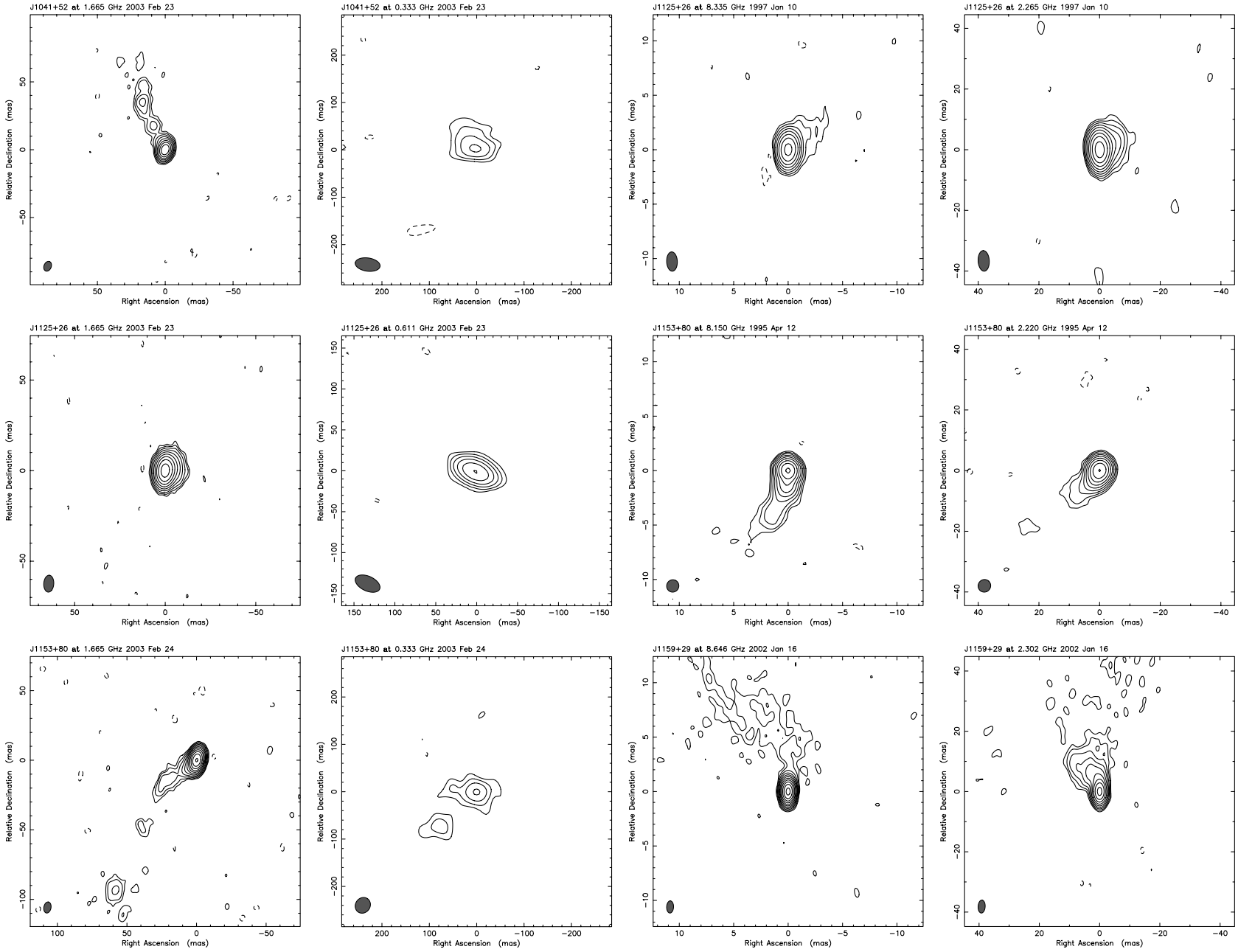

FIG. 1.—*Continued*

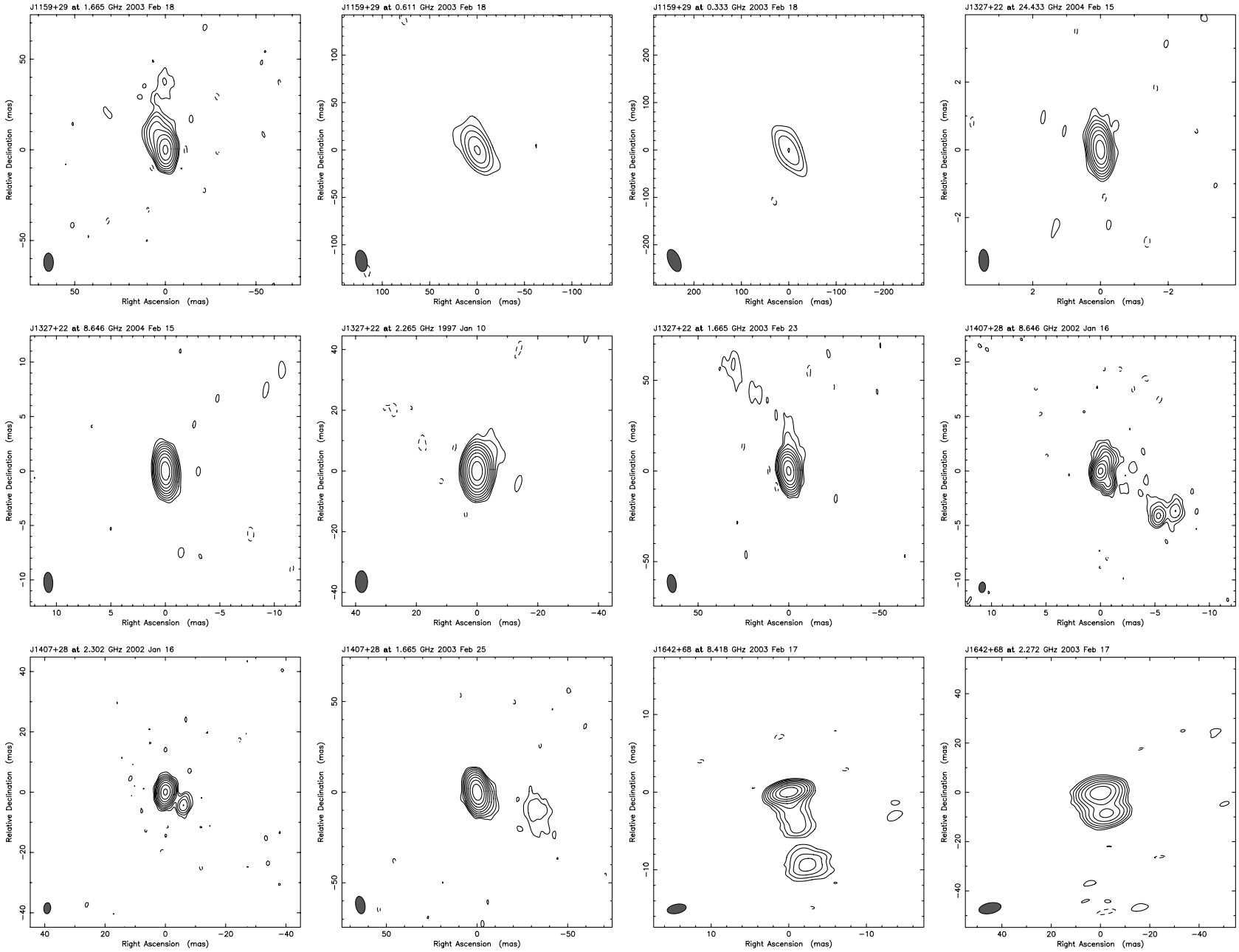

FIG. 1.—*Continued*

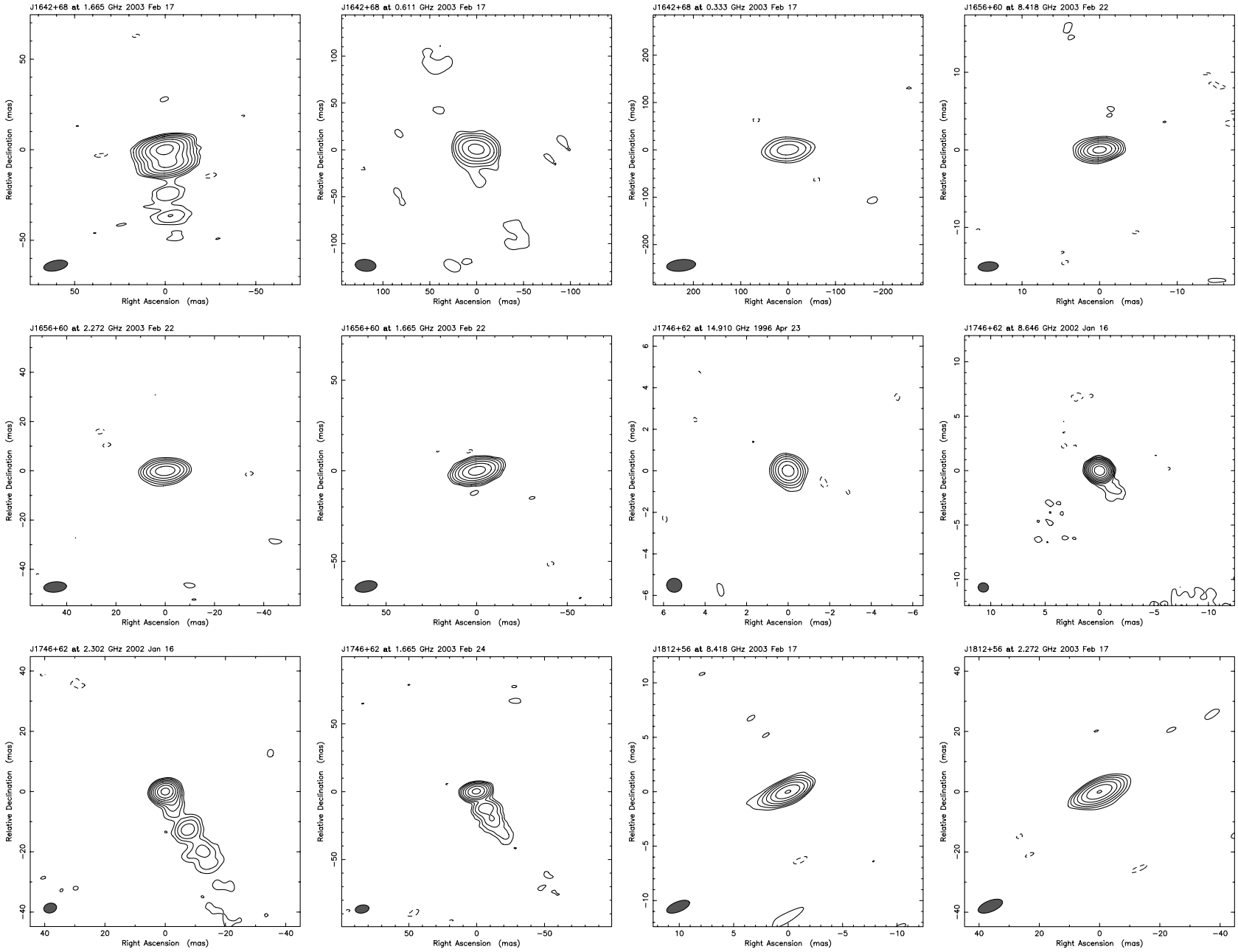

FIG. 1.—*Continued*

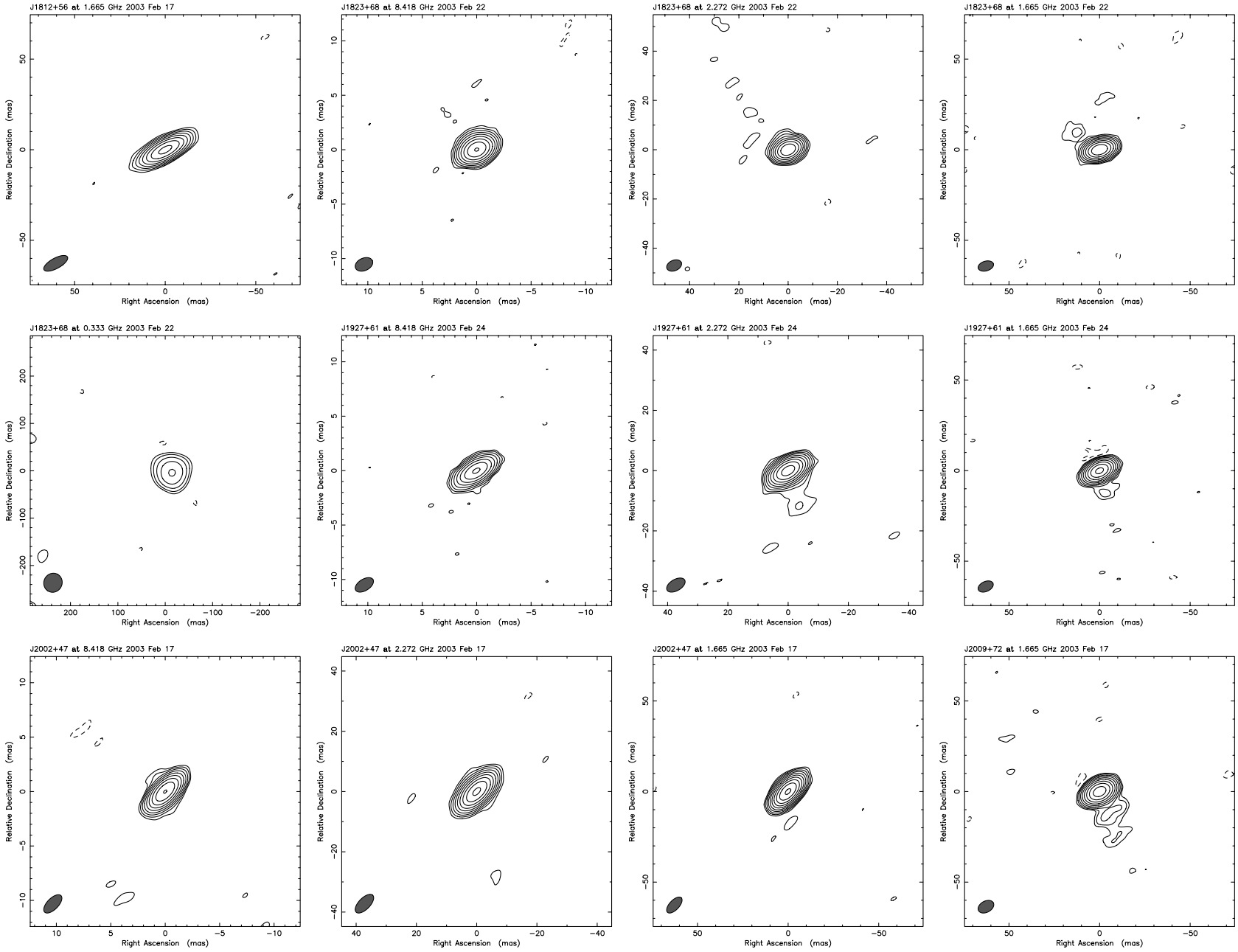

FIG. 1.—*Continued*

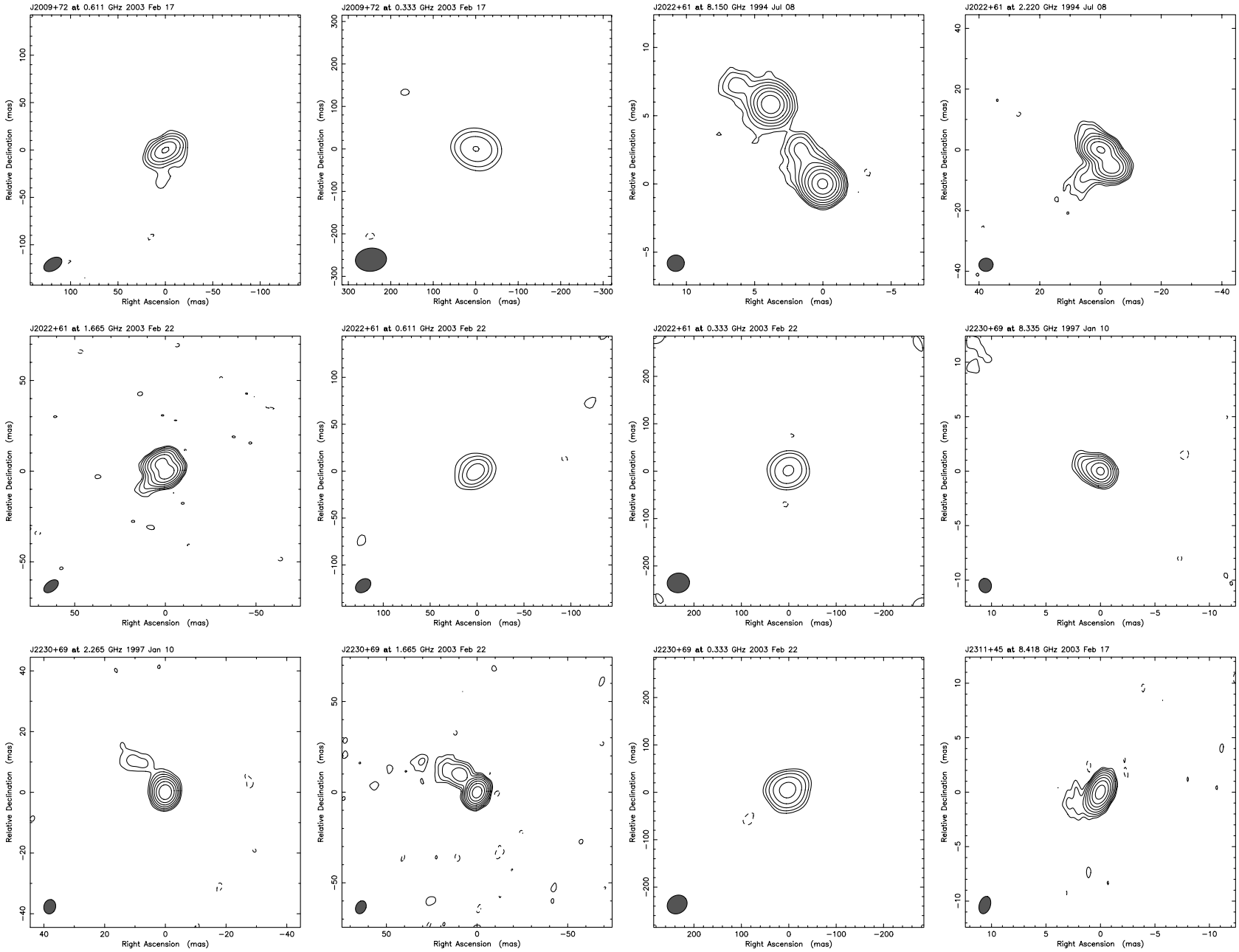

FIG. 1.—*Continued*

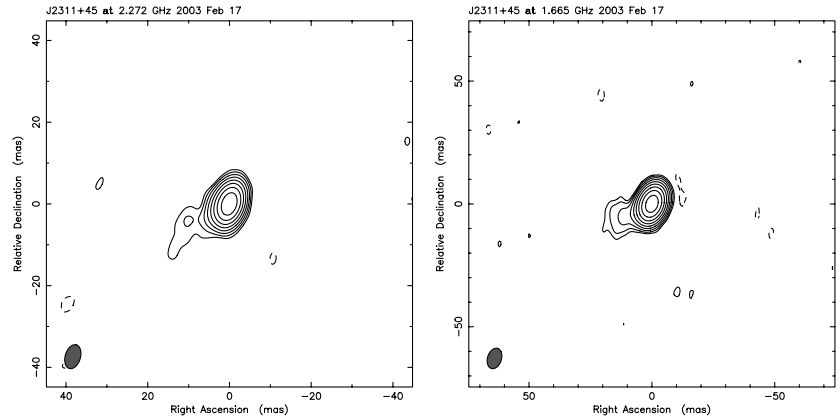

FIG. 1.—*Continued*

TABLE 2
PARAMETERS OF NATURALLY WEIGHTED IMAGES

SOURCE	ν (GHz)	BEAM[a] a (mas)	b (mas)	ϕ (deg)	PEAK (Jy beam^{-1})	rms[b] (mJy beam^{-1})	CONTOUR LEVELS[c] (mJy beam^{-1})
J0102+5824	24	0.7	0.3	36	2.13	2.5	$7.6 \times (1, \ldots, 2^8)$
	8.4	0.8	0.6	29	1.33	0.4	$1.2 \times (1, \ldots, 2^{10})$
	2.3	3.3	2.5	32	0.57	0.5	$1.2 \times (1, \ldots, 2^8)$
	1.6	7.1	5.1	10	1.12	1.1	$3.2 \times (1, \ldots, 2^8)$
	0.61	19.3	11.9	2	0.33	6.7	$20.2 \times (1, \ldots, 2^4)$
J0217+7349	24	0.5	0.4	89	0.71	1.8	$5.4 \times (1, \ldots, 2^7)$
	8.4	1.3	0.9	−77	2.24	0.9	$2.6 \times (1, \ldots, 2^9)$
	2.3	4.6	4.2	31	1.82	1.4	$4.1 \times (1, \ldots, 2^8)$
	1.6	6.6	5.5	20	1.30	1.0	$3.1 \times (1, \ldots, 2^8)$
	0.61	14.8	12.5	9	1.07	10.4	$31.3 \times (1, \ldots, 2^5)$
J0343+3622	24	0.7	0.3	−16	0.27	1.3	$4.0 \times (1, \ldots, 2^6)$
	1.6	7.7	6.1	−5	0.25	0.4	$1.2 \times (1, \ldots, 2^7)$
	0.33	46.7	34.6	30	0.11	4.4	$11.8 \times (1, \ldots, 2^3)$
J0349+4609	8.4	1.5	1.1	−3	0.43	0.9	$2.8 \times (1, \ldots, 2^7)$
	2.3	5.3	3.8	−3	0.53	0.8	$2.5 \times (1, \ldots, 2^7)$
	1.6	7.3	5.6	−11	0.53	1.4	$4.2 \times (1, \ldots, 2^6)$
	0.33	39.2	30.7	35	0.29	9.8	$25.4 \times (1, \ldots, 2^3)$
J0403+2600	8.4	1.8	1.1	−4	0.41	1.4	$4.2 \times (1, \ldots, 2^6)$
	2.3	6.8	3.8	−4	0.62	1.6	$4.7 \times (1, \ldots, 2^7)$
	1.6	9.4	5.6	7	0.47	0.6	$1.7 \times (1, \ldots, 2^8)$
	0.61	33.5	15.1	34	0.63	6.3	$19.0 \times (1, \ldots, 2^5)$
	0.33	61.3	28.3	35	0.24	7.6	$19.1 \times (1, \ldots, 2^3)$
J0419+3955	24	0.8	0.3	−36	0.30	1.8	$5.3 \times (1, \ldots, 2^5)$
	1.6	7.5	6.0	−9	0.35	0.3	$0.8 \times (1, \ldots, 2^8)$
	0.33	42.7	35.0	33	0.16	3.8	$8.7 \times (1, \ldots, 2^4)$
J0423+4150	8.4	1.4	1.3	−21	0.28	1.0	$3.1 \times (1, \ldots, 2^6)$
	2.3	5.3	3.7	−9	1.00	1.1	$3.3 \times (1, \ldots, 2^8)$
	1.6	7.7	6.2	4	0.88	0.8	$2.4 \times (1, \ldots, 2^8)$
J0451+5935	8.4	1.3	1.2	0	0.29	0.7	$2.2 \times (1, \ldots, 2^7)$
	2.3	4.8	4.2	1	0.30	0.8	$2.2 \times (1, \ldots, 2^7)$
	1.6	6.5	6.3	62	0.25	0.6	$1.8 \times (1, \ldots, 2^7)$
J0502+1338	24	0.8	0.4	10	0.31	2.4	$6.7 \times (1, \ldots, 2^5)$
	1.6	9.5	5.9	−5	0.34	0.8	$2.4 \times (1, \ldots, 2^7)$
	0.33	55.8	33.3	23	0.14	2.8	$8.4 \times (1, \ldots, 2^4)$
J0503+0203	8.4	2.1	0.9	−4	0.41	0.9	$2.7 \times (1, \ldots, 2^7)$
	2.3	7.6	3.4	−3	1.68	1.3	$3.8 \times (1, \ldots, 2^8)$
	1.6	11.0	5.7	7	1.50	2.0	$6.1 \times (1, \ldots, 2^7)$
	0.61	25.3	12.1	−1	0.64	17.5	$47.3 \times (1, \ldots, 2^3)$
J0507+4645	1.6	8.0	6.4	−16	0.51	0.9	$2.6 \times (1, \ldots, 2^7)$
	0.61	16.8	15.7	−32	0.54	10.7	$32.2 \times (1, \ldots, 2^4)$
	0.33	65.9	60.5	17	0.28	13.5	$37.7 \times (1, \ldots, 2^2)$
J0509+0541	24	1.0	0.4	−22	0.31	3.5	$10.5 \times (1, \ldots, 2^4)$
	1.6	11.0	6.0	−6	0.50	0.8	$2.3 \times (1, \ldots, 2^7)$
	0.61	25.8	13.5	−5	0.28	5.5	$16.6 \times (1, \ldots, 2^4)$
	0.33	62.7	34.8	20	0.26	6.8	$15.6 \times (1, \ldots, 2^4)$
J0539+1433	8.4	1.9	1.1	6	0.90	1.2	$3.6 \times (1, \ldots, 2^7)$
	2.3	7.2	4.1	5	0.92	0.9	$2.8 \times (1, \ldots, 2^8)$
	1.6	9.7	5.0	−3	0.88	0.7	$2.2 \times (1, \ldots, 2^8)$
J0607+6720	8.4	1.2	1.1	21	0.57	0.9	$2.8 \times (1, \ldots, 2^7)$
	2.3	4.4	4.2	20	0.82	0.9	$2.6 \times (1, \ldots, 2^8)$
	1.6	6.4	6.0	−87	0.79	0.4	$1.3 \times (1, \ldots, 2^9)$
	0.61	16.1	14.0	−86	0.58	6.3	$16.9 \times (1, \ldots, 2^5)$
	0.33	50.0	36.3	76	0.19	7.7	$19.2 \times (1, \ldots, 2^3)$

TABLE 2—*Continued*

Source	ν (GHz)	Beam[a] a (mas)	Beam[a] b (mas)	Beam[a] ϕ (deg)	Peak (Jy beam^{-1})	rms[b] (mJy beam^{-1})	Contour Levels[c] (mJy beam^{-1})
J0650+6001	8.4	1.3	1.1	31	0.46	1.2	$3.5 \times (1, \ldots, 2^7)$
	2.3	4.7	4.1	32	0.60	1.0	$3.0 \times (1, \ldots, 2^7)$
	1.6	6.6	6.2	−39	0.46	0.6	$1.9 \times (1, \ldots, 2^7)$
J0654+5042	8.4	1.4	1.1	13	0.26	0.6	$1.6 \times (1, \ldots, 2^7)$
	2.3	5.3	4.0	11	0.31	0.7	$2.0 \times (1, \ldots, 2^7)$
	1.6	7.1	5.9	11	0.29	0.5	$1.6 \times (1, \ldots, 2^7)$
J0713+4349	8.4	1.7	1.5	55	0.30	1.8	$6.3 \times (1, \ldots, 2^5)$
	2.3	5.8	4.8	35	1.19	2.0	$6.0 \times (1, \ldots, 2^7)$
	1.6	7.0	6.2	−13	1.02	1.7	$5.2 \times (1, \ldots, 2^7)$
	0.61	20.3	13.8	−7	0.86	20.6	$47.4 \times (1, \ldots, 2^4)$
	0.33	42.5	37.4	15	0.38	6.4	$15.9 \times (1, \ldots, 2^4)$
J0721+7120	8.4	1.4	1.1	7	0.21	1.8	$4.8 \times (1, \ldots, 2^5)$
	2.3	4.9	3.8	7	0.26	2.4	$6.8 \times (1, \ldots, 2^5)$
	1.6	6.5	5.9	−61	0.30	0.4	$1.3 \times (1, \ldots, 2^7)$
J0725+1425	8.4	1.8	1.2	9	0.88	1.1	$3.4 \times (1, \ldots, 2^8)$
	2.3	6.8	4.3	10	0.53	1.0	$2.7 \times (1, \ldots, 2^7)$
	1.6	9.0	6.0	1	0.50	1.7	$5.0 \times (1, \ldots, 2^6)$
	0.33	52.0	33.5	26	0.28	14.1	$35.3 \times (1, \ldots, 2^2)$
J0738+1742	15	3.9	1.5	47	0.92	4.4	$12.4 \times (1, \ldots, 2^6)$
	8.4	1.8	1.0	0	0.36	0.9	$2.8 \times (1, \ldots, 2^6)$
	2.3	6.6	3.5	−1	1.05	1.1	$3.3 \times (1, \ldots, 2^8)$
	1.6	9.2	6.8	−2	1.06	2.3	$7.0 \times (1, \ldots, 2^7)$
	0.33	47.7	28.6	26	0.49	16.6	$44.7 \times (1, \ldots, 2^3)$
J0745+1011	15	1.6	0.5	−23	0.66	11.9	$31.1 \times (1, \ldots, 2^4)$
	8.4	2.0	1.0	3	1.19	1.6	$4.9 \times (1, \ldots, 2^7)$
	2.3	7.4	3.8	3	3.10	4.0	$11.9 \times (1, \ldots, 2^8)$
	1.6	10.2	5.5	3	2.83	2.7	$8.0 \times (1, \ldots, 2^8)$
	0.61	23.7	13.1	1	0.98	10.2	$29.5 \times (1, \ldots, 2^5)$
	0.33	44.7	24.7	3	0.26	10.0	$28.0 \times (1, \ldots, 2^3)$
J0757+0956	24	0.7	0.3	−3	1.17	2.4	$7.2 \times (1, \ldots, 2^7)$
	8.4	2.0	0.8	−2	1.18	1.3	$3.8 \times (1, \ldots, 2^8)$
	2.3	7.0	3.5	0	1.48	1.2	$3.5 \times (1, \ldots, 2^8)$
	1.6	9.9	5.9	0	0.88	0.7	$2.0 \times (1, \ldots, 2^8)$
	0.33	51.7	36.7	28	0.22	11.3	$24.8 \times (1, \ldots, 2^3)$
J0808+4950	24	0.7	0.3	6	0.52	1.7	$5.0 \times (1, \ldots, 2^6)$
	8.4	1.8	0.8	0	0.59	1.0	$2.9 \times (1, \ldots, 2^7)$
	2.3	3.0	2.3	11	0.49	0.5	$1.4 \times (1, \ldots, 2^8)$
	1.6	7.0	6.3	−51	0.59	0.4	$1.3 \times (1, \ldots, 2^8)$
J0830+2410	8.4	1.8	1.0	8	0.97	0.9	$2.6 \times (1, \ldots, 2^8)$
	2.3	6.8	3.7	8	0.68	1.1	$3.2 \times (1, \ldots, 2^7)$
	1.6	9.3	5.5	1	0.61	0.9	$2.8 \times (1, \ldots, 2^7)$
	0.61	20.7	12.8	1	0.55	5.7	$14.7 \times (1, \ldots, 2^5)$
	0.33	39.3	24.4	3	0.23	7.1	$19.8 \times (1, \ldots, 2^3)$
J0831+0429	8.4	1.9	0.9	−2	0.49	1.0	$2.6 \times (1, \ldots, 2^7)$
	2.3	7.2	3.4	−1	0.79	1.1	$3.0 \times (1, \ldots, 2^8)$
	1.6	10.7	5.2	−2	0.67	1.6	$4.9 \times (1, \ldots, 2^7)$
	0.61	25.6	14.6	2	0.46	11.8	$35.5 \times (1, \ldots, 2^3)$
	0.33	55.5	32.4	17	0.23	14.6	$36.4 \times (1, \ldots, 2^2)$
J0842+1835	15	1.1	0.5	−20	0.26	5.5	$13.8 \times (1, \ldots, 2^4)$
	8.4	1.2	0.6	−11	0.27	1.9	$5.7 \times (1, \ldots, 2^5)$
	2.3	4.8	3.1	1	0.44	1.4	$4.5 \times (1, \ldots, 2^6)$
	1.6	9.1	5.9	−10	0.62	1.0	$3.1 \times (1, \ldots, 2^7)$
	0.33	46.5	28.2	26	0.38	16.5	$41.3 \times (1, \ldots, 2^3)$

TABLE 2—*Continued*

Source	ν (GHz)	Beam[a] a (mas)	Beam[a] b (mas)	Beam[a] ϕ (deg)	Peak (Jy beam^{-1})	rms[b] (mJy beam^{-1})	Contour Levels[c] (mJy beam^{-1})
J0914+0245	24	1.4	0.3	−18	0.89	1.6	$4.5 \times (1, \ldots, 2^7)$
	8.4	2.1	1.0	−3	0.46	1.4	$3.8 \times (1, \ldots, 2^6)$
	2.3	7.8	3.5	−2	0.50	2.8	$7.8 \times (1, \ldots, 2^5)$
	1.6	10.9	5.2	6	0.22	1.2	$3.5 \times (1, \ldots, 2^5)$
J0920+4441	8.4	1.4	1.0	4	0.54	1.0	$3.1 \times (1, \ldots, 2^7)$
	2.3	5.5	3.8	6	1.17	1.2	$3.5 \times (1, \ldots, 2^8)$
	1.6	7.3	5.7	−11	0.83	0.6	$1.9 \times (1, \ldots, 2^8)$
	0.33	42.9	30.1	67	0.35	7.8	$23.5 \times (1, \ldots, 2^3)$
J0956+2515	24	0.6	0.3	−3	0.47	1.4	$4.1 \times (1, \ldots, 2^6)$
	8.4	1.8	0.8	−3	0.37	1.1	$3.2 \times (1, \ldots, 2^6)$
	2.3	6.4	2.8	−8	1.07	1.4	$4.0 \times (1, \ldots, 2^8)$
	1.6	9.0	5.8	−4	0.83	0.6	$1.7 \times (1, \ldots, 2^8)$
	0.61	20.9	12.5	3	0.55	7.0	$17.6 \times (1, \ldots, 2^4)$
J0958+4725	15	1.6	0.9	−67	1.28	3.5	$8.8 \times (1, \ldots, 2^7)$
	8.4	1.1	0.7	−6	1.33	0.8	$2.5 \times (1, \ldots, 2^9)$
	2.3	4.3	2.9	0	0.88	1.0	$2.7 \times (1, \ldots, 2^8)$
	1.6	7.4	5.7	−2	0.95	0.7	$2.0 \times (1, \ldots, 2^8)$
	0.33	42.0	29.5	78	0.15	4.8	$13.8 \times (1, \ldots, 2^3)$
J1008+0621	24	1.4	0.3	−20	0.36	1.8	$5.1 \times (1, \ldots, 2^6)$
	1.6	10.4	5.3	2	0.42	1.2	$3.7 \times (1, \ldots, 2^6)$
	0.61	25.0	12.5	1	0.29	10.9	$28.4 \times (1, \ldots, 2^3)$
J1014+2301	8.4	1.8	1.0	12	0.64	1.1	$3.2 \times (1, \ldots, 2^7)$
	2.3	6.8	3.8	11	0.41	1.0	$3.1 \times (1, \ldots, 2^7)$
	1.6	9.1	5.7	−3	0.33	0.6	$1.9 \times (1, \ldots, 2^7)$
J1041+5233	8.4	1.5	1.1	27	0.33	1.0	$3.0 \times (1, \ldots, 2^6)$
	2.3	5.4	4.1	40	0.38	1.0	$2.8 \times (1, \ldots, 2^7)$
	1.6	7.5	5.4	−22	0.34	0.5	$1.4 \times (1, \ldots, 2^7)$
	0.33	53.0	28.0	82	0.13	4.8	$14.4 \times (1, \ldots, 2^3)$
J1125+2610	8.4	1.8	1.0	2	0.47	0.9	$2.8 \times (1, \ldots, 2^7)$
	2.3	6.8	3.7	3	1.06	1.0	$2.7 \times (1, \ldots, 2^8)$
	1.6	9.3	5.5	−4	0.73	0.6	$1.9 \times (1, \ldots, 2^8)$
	0.61	32.4	17.9	65	0.76	8.4	$23.7 \times (1, \ldots, 2^5)$
J1153+8058	8.4	1.1	1.1	−23	0.90	1.1	$3.2 \times (1, \ldots, 2^8)$
	2.3	4.2	4.1	−40	1.25	1.6	$4.8 \times (1, \ldots, 2^8)$
	1.6	8.0	5.2	−11	1.40	0.4	$1.3 \times (1, \ldots, 2^{10})$
	0.33	34.4	30.9	−36	0.28	11.9	$32.2 \times (1, \ldots, 2^3)$
J1159+2914	8.4	1.1	0.6	−2	2.59	0.7	$2.0 \times (1, \ldots, 2^{10})$
	2.3	4.3	2.3	−3	0.75	0.8	$2.3 \times (1, \ldots, 2^8)$
	1.6	10.1	5.3	1	1.21	2.7	$8.1 \times (1, \ldots, 2^7)$
	0.61	22.7	12.1	9	0.88	20.8	$49.8 \times (1, \ldots, 2^4)$
	0.33	49.5	24.5	23	0.39	16.0	$48.1 \times (1, \ldots, 2^3)$
J1327+2210	24	0.6	0.3	3	1.12	1.8	$5.5 \times (1, \ldots, 2^7)$
	8.4	1.9	0.8	3	1.04	0.8	$2.3 \times (1, \ldots, 2^8)$
	2.3	7.1	4.0	1	1.97	1.5	$4.5 \times (1, \ldots, 2^8)$
	1.6	10.1	4.9	8	0.77	0.9	$2.6 \times (1, \ldots, 2^8)$
J1407+2827	8.4	1.0	0.6	−6	0.77	0.8	$2.5 \times (1, \ldots, 2^8)$
	2.3	3.7	2.3	−6	0.93	1.0	$3.0 \times (1, \ldots, 2^8)$
	1.6	9.7	5.1	10	0.89	0.7	$2.0 \times (1, \ldots, 2^8)$
J1642+6856	8.4	2.5	1.2	−78	0.82	1.2	$3.4 \times (1, \ldots, 2^7)$
	2.3	9.1	4.3	−79	0.46	1.3	$3.9 \times (1, \ldots, 2^6)$
	1.6	13.4	5.6	−79	0.42	0.8	$2.4 \times (1, \ldots, 2^7)$
	0.61	22.2	12.7	85	0.61	6.2	$13.7 \times (1, \ldots, 2^5)$
	0.33	61.4	24.6	−84	0.31	9.7	$26.1 \times (1, \ldots, 2^3)$

TABLE 2—*Continued*

Source	ν (GHz)	Beam[a] a (mas)	Beam[a] b (mas)	Beam[a] ϕ (deg)	Peak (Jy beam^{-1})	rms[b] (mJy beam^{-1})	Contour Levels[c] (mJy beam^{-1})
J1656+6012	8.4	2.6	1.2	−85	0.19	0.8	$2.2 \times (1, \ldots, 2^6)$
	2.3	9.3	4.2	−85	0.18	1.3	$3.4 \times (1, \ldots, 2^5)$
	1.6	12.3	6.0	−79	0.16	0.6	$1.7 \times (1, \ldots, 2^6)$
J1746+6226	15	0.7	0.7	82	0.39	2.9	$8.1 \times (1, \ldots, 2^5)$
	8.4	1.0	0.9	83	0.56	0.4	$1.2 \times (1, \ldots, 2^8)$
	2.3	4.3	3.2	−76	0.22	0.4	$1.3 \times (1, \ldots, 2^7)$
	1.6	10.3	6.0	−80	0.19	0.8	$2.3 \times (1, \ldots, 2^6)$
J1812+5603	8.4	2.2	0.9	−68	0.20	1.1	$3.1 \times (1, \ldots, 2^6)$
	2.3	8.6	3.7	−68	0.25	1.3	$3.8 \times (1, \ldots, 2^6)$
	1.6	14.8	5.7	−61	0.22	0.5	$1.4 \times (1, \ldots, 2^7)$
J1823+6857	8.4	1.7	1.1	−66	0.60	0.8	$2.3 \times (1, \ldots, 2^8)$
	2.3	6.3	4.3	−67	0.60	0.9	$2.4 \times (1, \ldots, 2^7)$
	1.6	8.7	5.4	−74	0.53	0.7	$2.1 \times (1, \ldots, 2^7)$
	0.33	40.7	38.5	−28	0.17	4.1	$9.9 \times (1, \ldots, 2^4)$
J1927+6117	8.4	1.9	1.0	−58	1.16	2.8	$8.4 \times (1, \ldots, 2^7)$
	2.3	6.7	3.8	−60	1.40	1.4	$3.9 \times (1, \ldots, 2^8)$
	1.6	8.9	5.5	−65	1.23	1.3	$4.0 \times (1, \ldots, 2^8)$
J2002+4725	8.4	2.1	1.0	−45	0.57	0.7	$2.2 \times (1, \ldots, 2^8)$
	2.3	7.9	3.8	−44	0.68	0.8	$2.3 \times (1, \ldots, 2^8)$
	1.6	11.0	5.3	−43	0.58	0.3	$1.0 \times (1, \ldots, 2^9)$
J2009+7229	1.6	9.2	6.2	−62	1.18	1.0	$3.0 \times (1, \ldots, 2^8)$
	0.61	20.9	12.5	−59	0.76	7.1	$21.4 \times (1, \ldots, 2^5)$
	0.33	73.4	54.6	−84	0.22	9.0	$27.1 \times (1, \ldots, 2^3)$
J2022+6136	8.4	1.3	1.2	−83	1.75	1.8	$5.5 \times (1, \ldots, 2^8)$
	2.3	4.7	4.4	−86	1.10	2.4	$7.5 \times (1, \ldots, 2^7)$
	1.6	9.3	5.5	−52	0.91	2.8	$8.4 \times (1, \ldots, 2^6)$
	0.61	18.0	13.0	−53	0.85	23.8	$59.4 \times (1, \ldots, 2^3)$
	0.33	47.3	41.4	−81	0.40	17.1	$44.4 \times (1, \ldots, 2^3)$
J2230+6946	8.4	1.3	1.1	12	0.19	0.9	$2.4 \times (1, \ldots, 2^6)$
	2.3	4.8	3.9	−14	0.39	1.1	$3.1 \times (1, \ldots, 2^6)$
	1.6	7.5	5.5	−27	0.24	0.4	$1.1 \times (1, \ldots, 2^7)$
	0.33	44.0	37.6	−56	0.20	3.2	$8.9 \times (1, \ldots, 2^4)$
J2311+4543	8.4	1.6	1.0	−18	0.41	0.7	$2.1 \times (1, \ldots, 2^7)$
	2.3	6.0	3.7	−17	0.47	0.7	$2.0 \times (1, \ldots, 2^7)$
	1.6	8.6	5.7	−18	0.42	0.3	$1.0 \times (1, \ldots, 2^8)$

Note.—Table 2 is also available in machine-readable form in the electronic edition of the *Astrophysical Journal Supplement*.

[a] The restoring beam is an elliptical Gaussian with FWHM major axis a and minor axis b, with major axis in position angle ϕ (measured north through east).

[b] The root mean square (rms) of the residuals of the final hybrid image.

[c] Contour levels are represented by the geometric series $1, \ldots, 2^n$, e.g., for $n = 5$ the contour levels would be ± 1, 2, 4, 8, 16, and 32.

TABLE 3
GAUSSIAN MODELS

Source	ν (GHz)	Comp. Number	S (Jy)	r (mas)	θ (deg)	a (mas)	b/a	ϕ (deg)
J0102+5824	24	1	1.48	0.0	...	0.07	1.00	...
		2	1.25	0.2	173	0.24	1.00	...
	8.4	1	1.37	0.0	...	0.13	1.00	...
		2	0.02	0.7	−123	0.44	1.00	...
		3	0.03	1.5	−132	0.98	1.00	...
	2.3	1	0.62	0.0	...	1.11	0.76	−24
		2	0.07	2.2	−118	1.53	1.00	...
		3	0.02	5.3	−112	3.09	1.00	...
		4	0.01	13.4	−94	2.83	1.00	...
	1.6	1	1.20	0.0	...	2.39	0.51	−39
		2	0.07	3.2	−118	2.02	1.00	...
		3	0.02	6.8	−105	3.37	1.00	...
		4	0.01	17.6	−91	8.74	1.00	...
	0.61	1	0.51	0.0	...	13.40	0.54	−45
J0217+7349	24	1	1.11	0.0	...	0.41	0.64	60
		2	0.22	0.7	−65	0.24	1.00	...
		3	0.24	1.1	−66	0.12	1.00	...
	8.4	1	2.30	0.0	...	0.51	0.74	85
		2	0.54	0.8	−64	0.29	0.20	−86
		3	0.04	1.2	100	0.21	1.00	...
		4	0.07	2.5	102	1.03	1.00	...
		5	0.02	5.6	102	0.97	1.00	...
		6	0.08	13.7	91	1.81	1.00	...
	2.3	1	1.22	0.0	...	0.27	1.00	...
		2	0.85	1.9	103	0.65	1.00	...
		3	0.29	5.7	102	2.19	1.00	...
		4	0.59	13.6	91	2.38	1.00	...
	1.6	1	1.24	0.0	...	1.34	1.00	...
		2	0.40	3.8	105	2.71	1.00	...
		3	0.52	13.2	91	3.10	1.00	...
	0.61	1	1.86	0.0	...	15.42	0.30	88
J0343+3622	24	1	0.26	0.0	...	0.08	1.00	...
		2	0.04	0.2	29	0.15	1.00	...
	1.6	1	0.27	0.0	...	2.12	1.00	...
		2	0.02	10.4	−6	12.72	1.00	...
	0.33	1	0.24	0.0	...	58.62	0.45	54
J0349+4609	8.4	1	0.46	0.0	...	0.43	0.21	−69
		2	0.10	2.3	130	1.63	1.00	...
	2.3	1	0.45	0.0	...	0.61	1.00	...
		2	0.16	2.2	131	1.72	1.00	...
		3	0.04	4.3	142	7.87	1.00	...
		4	0.05	22.6	137	12.91	1.00	...
	1.6	1	0.19	0.0	...	2.79	1.00	...
		2	0.42	2.5	−41	1.08	1.00	...
		3	0.17	15.5	144	23.13	1.00	...
	0.33	1	0.44	0.0	...	29.73	0.67	−18
J0403+2600	8.4	1	0.43	0.0	...	0.31	1.00	...
		2	0.12	1.3	85	1.30	1.00	...
		3	0.17	4.9	46	3.24	1.00	...
	2.3	1	0.51	0.0	...	1.31	1.00	...
		2	0.25	2.3	60	1.55	1.00	...
		3	0.19	5.5	36	1.37	1.00	...
		4	0.09	8.7	31	4.95	1.00	...
	1.6	1	0.18	0.0	...	2.13	1.00	...
		2	0.30	3.2	−129	1.43	1.00	...
		3	0.18	3.6	23	2.48	1.00	...
		4	0.06	8.8	28	5.72	1.00	...
		5	0.01	21.7	25	6.96	1.00	...
		6	0.02	43.4	24	16.65	1.00	...
	0.61	1	0.73	0.0	...	17.24	0.24	41
	0.33	1	0.32	0.0	...	46.45	0.29	38
J0419+3955	24	1	0.35	0.0	...	0.29	0.47	−64
	1.6	1	0.35	0.0	...	0.98	1.00	...
		2	0.01	0.6	−154	8.47	1.00	...
	0.33	1	0.19	0.0	...	27.93	0.00	45

TABLE 3—*Continued*

Source	ν (GHz)	Comp. Number	S (Jy)	r (mas)	θ (deg)	a (mas)	b/a	ϕ (deg)
J0423+4150	8.4	1	0.34	0.0	...	0.92	0.27	77
		2	0.04	2.1	76	0.73	0.00	−43
		3	0.27	2.4	−102	1.66	0.69	75
		4	0.01	5.6	−114	1.61	1.00	...
	2.3	1	0.75	0.0	...	1.06	1.00	...
		2	0.45	2.1	80	0.80	1.00	...
		3	0.22	2.4	−111	1.78	1.00	...
		4	0.06	11.3	−90	7.84	1.00	...
		5	0.02	23.9	−128	6.01	1.00	...
	1.6	1	0.57	0.0	...	1.47	1.00	...
		2	0.60	3.7	−107	2.36	1.00	...
		3	0.09	11.3	−98	9.42	1.00	...
J0451+5935	8.4	1	0.30	0.0	...	0.22	1.00	...
	2.3	1	0.31	0.0	...	0.76	1.00	...
		2	0.02	2.9	107	1.95	1.00	...
	1.6	1	0.28	0.0	...	2.21	1.00	...
J0502+1338	24	1	0.37	0.0	...	0.37	0.12	46
	1.6	1	0.29	0.0	...	1.29	1.00	...
		2	0.12	3.5	73	4.04	1.00	...
		3	0.02	17.8	98	18.78	1.00	...
	0.33	1	0.31	0.0	...	64.02	0.39	53
J0503+0203	8.4	1	0.48	0.0	...	0.96	0.23	−15
		2	0.07	2.0	−170	0.69	1.00	...
		3	0.32	2.2	−46	1.23	0.59	−38
		4	0.02	3.9	−51	0.45	1.00	...
		5	0.03	6.8	−164	0.33	1.00	...
		6	0.07	8.8	179	0.83	1.00	...
	2.3	1	1.05	0.0	...	0.80	1.00	...
		2	1.09	2.6	−42	1.27	1.00	...
		3	0.09	5.7	−44	3.70	1.00	...
		4	0.50	8.6	180	2.24	1.00	...
	1.6	1	1.76	0.0	...	4.39	0.44	−32
		2	0.03	6.9	−61	1.76	1.00	...
		3	0.44	10.1	173	2.33	1.00	...
	0.61	1	1.06	0.0	...	14.19	1.00	...
J0507+4645	1.6	1	0.35	0.0	...	1.87	1.00	...
		2	0.22	2.2	148	1.12	1.00	...
		3	0.01	15.3	−79	4.50	1.00	...
	0.61	1	0.59	0.0	...	7.48	0.35	−63
	0.33	1	0.32	0.0	...	25.75	1.00	...
J0509+0541	24	1	0.35	0.0	...	0.16	1.00	...
		2	0.04	1.0	−165	0.57	1.00	...
	1.6	1	0.40	0.0	...	1.04	1.00	...
		2	0.13	3.3	174	1.76	1.00	...
		3	0.02	9.4	171	11.21	1.00	...
	0.61	1	0.46	0.0	...	16.79	0.65	−64
	0.33	1	0.37	0.0	...	44.37	0.49	49
J0539+1433	8.4	1	0.95	0.0	...	0.40	0.76	39
	2.3	1	1.00	0.0	...	1.93	0.41	−42
	1.6	1	1.01	0.0	...	3.57	0.27	−46
		2	0.03	4.7	−45	6.60	1.00	...
J0607+6720	8.4	1	0.57	0.0	...	0.56	0.30	−11
		2	0.16	0.7	−174	0.64	1.00	...
	2.3	1	0.84	0.0	...	1.01	0.52	3
		2	0.05	2.5	−177	6.96	1.00	...
	1.6	1	0.79	0.0	...	0.90	1.00	...
		2	0.06	4.2	−179	5.26	1.00	...
	0.61	1	0.65	0.0	...	5.18	1.00	...
	0.33	1	0.21	0.0	...	13.83	1.00	...
J0650+6001	8.4	1	0.50	0.0	...	0.43	0.51	21
		2	0.04	1.9	−143	0.53	1.00	...
		3	0.21	3.0	−145	0.51	0.00	3
	2.3	1	0.45	0.0	...	1.22	1.00	...
		2	0.33	2.6	−146	0.92	1.00	...
	1.6	1	0.54	0.0	...	2.69	1.00	...

TABLE 3—*Continued*

Source	ν (GHz)	Comp. Number	S (Jy)	r (mas)	θ (deg)	a (mas)	b/a	ϕ (deg)
J0654+5042	8.4	1	0.24	0.0	...	0.17	1.00	...
		2	0.04	0.7	103	0.45	1.00	...
		3	0.03	1.5	99	0.77	1.00	...
	2.3	1	0.25	0.0	...	0.33	1.00	...
		2	0.08	1.1	97	1.96	1.00	...
	1.6	1	0.31	0.0	...	1.88	1.00	...
		2	0.01	4.0	121	1.13	1.00	...
J0713+4349	8.4	1	0.32	0.0	...	0.74	1.00	...
		2	0.18	1.4	−176	0.46	1.00	...
		3	0.05	6.6	5	1.14	1.00	...
		4	0.11	8.1	−8	1.08	1.00	...
		5	0.31	8.6	−1	0.61	1.00	...
		6	0.12	15.5	−177	1.29	1.00	...
	2.3	1	1.34	0.0	...	1.97	1.00	...
		2	0.11	4.0	−69	2.46	1.00	...
		3	0.75	7.9	177	1.32	1.00	...
		4	0.32	23.6	−179	1.65	1.00	...
	1.6	1	1.22	0.0	...	3.54	0.75	−48
		2	0.47	7.7	175	2.00	1.00	...
		3	0.23	23.4	−180	1.73	1.00	...
	0.61	1	1.12	0.0	...	11.78	0.51	−40
	0.33	1	0.43	0.0	...	20.94	0.00	88
J0721+7120	8.4	1	0.21	0.0	...	0.20	1.00	...
	2.3	1	0.27	0.0	...	0.52	1.00	...
	1.6	1	0.27	0.0	...	0.51	1.00	...
		2	0.05	2.6	16	1.35	1.00	...
		3	0.02	10.5	15	6.11	1.00	...
J0725+1425	8.4	1	0.84	0.0	...	0.18	1.00	...
		2	0.09	0.5	−57	0.33	1.00	...
		3	0.09	4.1	−66	2.70	1.00	...
	2.3	1	0.54	0.0	...	1.73	0.56	−48
		2	0.19	4.0	−66	2.65	1.00	...
		3	0.07	11.8	−106	7.35	1.00	...
		4	0.08	26.8	−130	20.99	1.00	...
	1.6	1	0.41	0.0	...	1.94	1.00	...
		2	0.29	4.0	−67	4.02	1.00	...
		3	0.08	14.1	−110	9.26	1.00	...
		4	0.06	30.1	−140	28.62	1.00	...
	0.33	1	0.28	0.0	...	16.77	1.00	...
		2	0.20	42.7	−107	29.96	1.00	...
J0738+1742	15	1	1.03	0.0	...	0.73	1.00	...
	8.4	1	0.27	0.0	...	0.24	1.00	...
		2	0.33	0.8	70	0.73	1.00	...
		3	0.04	3.7	64	1.99	1.00	...
	2.3	1	1.07	0.0	...	1.01	1.00	...
		2	0.12	3.0	65	2.26	1.00	...
		3	0.11	8.4	73	5.57	1.00	...
		4	0.07	15.6	74	6.71	1.00	...
		5	0.14	25.5	92	20.95	1.00	...
	1.6	1	1.13	0.0	...	2.00	1.00	...
		2	0.14	10.7	69	8.00	1.00	...
		3	0.15	23.8	84	16.73	1.00	...
	0.33	1	0.71	0.0	...	35.78	0.42	54
J0745+1011	15	1	0.53	0.0	...	0.22	1.00	...
		2	0.90	0.9	−17	1.73	1.00	...
	8.4	1	1.04	0.0	...	0.55	1.00	...
		2	0.51	0.8	151	0.40	1.00	...
		3	0.49	1.7	4	0.97	1.00	...
		4	0.06	3.0	40	1.02	1.00	...
	2.3	1	3.16	0.0	...	2.34	0.48	1
		2	0.44	2.1	89	3.98	1.00	...
		3	0.13	9.8	112	6.30	1.00	...
	1.6	1	2.44	0.0	...	1.09	1.00	...
		2	0.88	1.7	115	6.50	1.00	...
		3	0.13	11.4	125	7.02	1.00	...
	0.61	1	1.30	0.0	...	10.95	0.55	−61
	0.33	1	0.31	0.0	...	14.20	0.43	−61

TABLE 3—*Continued*

Source	ν (GHz)	Comp. Number	S (Jy)	r (mas)	θ (deg)	a (mas)	b/a	ϕ (deg)
J0757+0956	24	1	1.35	0.0	...	0.22	0.32	35
		2	0.29	1.3	20	0.77	0.40	−11
	8.4	1	1.10	0.0	...	0.15	1.00	...
		2	0.40	1.2	17	0.30	1.00	...
		3	0.07	3.4	15	1.22	1.00	...
	2.3	1	1.34	0.0	...	0.23	1.00	...
		2	0.25	3.1	11	1.13	1.00	...
	1.6	1	0.74	0.0	...	0.34	1.00	...
		2	0.20	3.3	11	1.73	1.00	...
		3	0.02	35.5	−9	20.76	1.00	...
	0.33	1	0.22	0.0	...	22.81	0.00	52
J0808+4950	24	1	0.57	0.0	...	0.12	0.81	60
	8.4	1	0.58	0.0	...	0.24	0.38	−42
		2	0.09	0.9	130	1.18	1.00	...
	2.3	1	0.38	0.0	...	0.41	1.00	...
		2	0.23	1.2	140	1.25	1.00	...
		3	0.03	4.1	159	2.23	1.00	...
	1.6	1	0.60	0.0	...	1.84	0.53	−26
		2	0.05	4.0	166	3.09	1.00	...
J0830+24	8.4	1	1.00	0.0	...	0.24	1.00	...
		2	0.13	1.4	115	0.45	1.00	...
		3	0.03	5.3	139	2.11	1.00	...
	2.3	1	0.75	0.0	...	1.91	0.00	−61
		2	0.09	4.5	136	1.89	1.00	...
		3	0.03	11.2	137	8.10	1.00	...
	1.6	1	0.36	0.0	...	1.04	1.00	...
		2	0.26	1.6	−52	0.91	1.00	...
		3	0.12	4.2	142	1.93	1.00	...
		4	0.02	11.0	149	5.63	1.00	...
		5	0.02	35.9	132	31.03	1.00	...
	0.61	1	0.62	0.0	...	7.88	0.30	−40
	0.33	1	0.27	0.0	...	11.71	1.00	...
J0831+0429	8.4	1	0.43	0.0	...	0.16	1.00	...
		2	0.13	0.6	61	0.00	1.00	...
		3	0.12	1.5	67	0.77	1.00	...
		4	0.06	2.9	67	1.31	1.00	...
		5	0.01	6.2	59	0.82	1.00	...
	2.3	1	0.72	0.0	...	0.86	1.00	...
		2	0.22	2.2	65	0.12	1.00	...
		3	0.08	4.8	61	0.49	1.00	...
		4	0.03	7.9	57	1.39	1.00	...
	1.6	1	0.72	0.0	...	2.16	1.00	...
		2	0.12	7.8	59	6.68	1.00	...
	0.61	1	0.84	0.0	...	20.83	0.38	−79
	0.33	1	0.34	0.0	...	63.99	0.00	72
J0842+1835	15	1	0.36	0.0	...	0.41	1.00	...
	8.4	1	0.35	0.0	...	0.74	0.34	14
		2	0.10	2.2	11	0.86	1.00	...
		3	0.10	12.0	15	0.84	1.00	...
	2.3	1	0.45	0.0	...	1.05	1.00	...
		2	0.09	3.4	16	1.21	1.00	...
		3	0.37	10.5	16	1.73	1.00	...
	1.6	1	0.65	0.0	...	2.09	1.00	...
		2	0.49	9.7	16	2.86	1.00	...
	0.33	1	0.47	0.0	...	41.12	0.00	33
J0914+0245	24	1	0.97	0.0	...	0.13	1.00	...
	8.4	1	0.46	0.0	...	0.12	1.00	...
		2	0.04	2.8	13	1.09	1.00	...
	2.3	1	0.48	0.0	...	0.47	1.00	...
		2	0.08	4.6	6	0.93	1.00	...
	1.6	1	0.11	0.0	...	2.96	1.00	...
		2	0.18	5.1	168	2.06	1.00	...

TABLE 3—*Continued*

Source	ν (GHz)	Comp. Number	S (Jy)	r (mas)	θ (deg)	a (mas)	b/a	ϕ (deg)
J0920+4441	8.4	1	0.51	0.0	...	0.63	0.12	−5
		2	0.30	1.1	178	0.45	1.00	...
	2.3	1	1.19	0.0	...	1.16	0.19	1
		2	0.06	5.6	−161	3.53	1.00	...
		3	0.07	19.3	−159	6.77	1.00	...
	1.6	1	0.81	0.0	...	0.84	1.00	...
		2	0.10	4.4	−165	4.27	1.00	...
		3	0.10	17.8	−158	9.69	1.00	...
	0.33	1	0.44	0.0	...	20.70	0.69	−82
J0956+2515	24	1	0.49	0.0	...	0.12	0.53	41
		2	0.12	0.5	−124	0.41	1.00	...
		3	0.17	1.2	−118	0.62	1.00	...
	8.4	1	0.40	0.0	...	0.43	1.00	...
		2	0.31	1.0	−114	0.76	1.00	...
	2.3	1	1.14	0.0	...	1.03	1.00	...
		2	0.03	10.4	−93	3.33	1.00	...
	1.6	1	0.85	0.0	...	1.15	1.00	...
		2	0.04	7.6	−93	5.74	1.00	...
	0.61	1	0.58	0.0	...	3.45	1.00	...
J0958+4725	15	1	1.33	0.0	...	0.23	1.00	...
	8.4	1	1.34	0.0	...	0.24	0.40	−72
		2	0.12	0.1	134	0.83	1.00	...
	2.3	1	0.89	0.0	...	0.65	0.62	−53
		2	0.03	3.6	146	5.55	1.00	...
	1.6	1	0.97	0.0	...	1.30	0.00	−38
		2	0.03	7.4	143	3.91	1.00	...
	0.33	1	0.17	0.0	...	22.50	0.00	−67
J1008+0621	24	1	0.35	0.0	...	0.03	1.00	...
		2	0.04	0.7	152	0.35	1.00	...
	1.6	1	0.47	0.0	...	4.09	0.28	−20
	0.61	1	0.40	0.0	...	13.39	0.00	85
J1014+2301	8.4	1	0.69	0.0	...	0.37	1.00	...
		2	0.05	2.2	111	1.17	1.00	...
		3	0.01	4.6	115	0.89	1.00	...
	2.3	1	0.38	0.0	...	0.86	1.00	...
		2	0.13	2.5	111	2.26	1.00	...
		3	0.01	61.5	107	3.02	1.00	...
	1.6	1	0.27	0.0	...	1.10	1.00	...
		2	0.10	3.0	115	1.24	1.00	...
		3	0.03	8.4	118	7.49	1.00	...
		4	0.06	59.8	109	30.03	1.00	...
J1041+5233	8.4	1	0.36	0.0	...	0.75	0.00	10
		2	0.10	1.4	24	0.22	1.00	...
	2.3	1	0.40	0.0	...	1.67	0.34	19
		2	0.01	5.3	24	0.00	1.00	...
		3	0.02	19.5	25	9.85	1.00	...
		4	0.02	38.5	27	5.37	1.00	...
	1.6	1	0.35	0.0	...	0.91	1.00	...
		2	0.03	5.1	20	3.31	1.00	...
		3	0.02	20.7	27	11.38	1.00	...
		4	0.02	38.5	26	5.53	1.00	...
		5	0.02	54.4	20	19.01	1.00	...
	0.33	1	0.11	0.0	...	15.45	0.00	−63
		2	0.12	28.0	27	49.61	0.82	17
J1125+2610	8.4	1	0.29	0.0	...	0.16	1.00	...
		2	0.25	0.5	−54	0.31	1.00	...
		3	0.02	2.2	−51	1.94	1.00	...
	2.3	1	0.96	0.0	...	0.47	0.00	−32
		2	0.16	1.8	−56	1.25	1.00	...
		3	0.06	5.3	−65	3.92	1.00	...
	1.6	1	0.70	0.0	...	1.22	1.00	...
		2	0.14	3.7	−64	4.62	1.00	...
	0.61	1	0.80	0.0	...	6.91	0.15	−79

TABLE 3—*Continued*

Source	ν (GHz)	Comp. Number	S (Jy)	r (mas)	θ (deg)	a (mas)	b/a	ϕ (deg)
J1153+8058	8.4	1	0.96	0.0	...	0.33	1.00	...
		2	0.27	1.3	176	0.77	1.00	...
		3	0.09	3.6	163	1.93	1.00	...
	2.3	1	0.58	0.0	...	0.57	1.00	...
		2	0.76	1.5	−8	0.33	1.00	...
		3	0.19	2.5	152	1.32	1.00	...
		4	0.07	7.9	134	6.43	1.00	...
		5	0.02	29.5	125	8.51	1.00	...
	1.6	1	0.82	0.0	...	1.02	1.00	...
		2	0.68	2.2	−20	0.91	1.00	...
		3	0.08	5.1	136	5.03	1.00	...
		4	0.03	22.6	123	11.27	1.00	...
		5	0.01	60.2	143	7.43	1.00	...
		6	0.03	110.4	148	16.75	1.00	...
	0.33	1	0.37	0.0	...	24.79	0.00	65
		2	0.18	103.5	133	32.40	1.00	...
J1159+2914	8.4	1	2.66	0.0	...	0.19	0.60	26
		2	0.08	0.7	12	0.69	1.00	...
		3	0.04	3.9	−2	1.76	1.00	...
		4	0.06	7.9	23	4.62	1.00	...
	2.3	1	0.83	0.0	...	1.57	0.46	27
		2	0.10	4.2	−2	2.43	1.00	...
		3	0.10	6.7	23	3.57	1.00	...
		4	0.16	10.1	25	9.45	1.00	...
	1.6	1	1.27	0.0	...	1.89	1.00	...
		2	0.31	8.5	29	6.82	1.00	...
		3	0.06	31.9	4	20.36	1.00	...
	0.61	1	1.32	0.0	...	17.95	0.27	40
	0.33	1	0.66	0.0	...	46.26	0.36	35
J1327+2210	24	1	0.93	0.0	...	0.03	1.00	...
		2	0.33	0.2	30	0.15	1.00	...
	8.4	1	0.88	0.0	...	0.23	0.33	19
		2	0.23	0.1	−55	0.59	1.00	...
	2.3	1	1.96	0.0	...	0.79	0.00	−19
		2	0.03	2.4	−87	2.23	1.00	...
		3	0.02	8.5	−32	3.53	1.00	...
	1.6	1	0.67	0.0	...	0.86	0.00	21
		2	0.14	0.9	−75	3.99	1.00	...
		3	0.02	7.5	−19	2.93	1.00	...
		4	0.01	18.4	−3	6.91	1.00	...
		5	0.01	44.3	23	14.86	1.00	...
		6	0.01	65.7	28	7.87	1.00	...
J1407+2827	8.4	1	1.12	0.0	...	0.59	0.76	−32
		2	0.17	1.2	−27	0.62	1.00	...
		3	0.13	1.3	−147	0.23	1.00	...
		4	0.06	6.7	−128	0.34	1.00	...
		5	0.04	7.7	−118	0.69	1.00	...
	2.3	1	1.33	0.0	...	2.30	0.70	−6
		2	0.06	7.3	−125	1.38	1.00	...
	1.6	1	0.96	0.0	...	2.08	1.00	...
		2	0.05	4.1	−142	8.89	1.00	...
		3	0.02	34.5	−108	10.80	1.00	...
J1642+6856	8.4	1	0.84	0.0	...	0.27	1.00	...
		2	0.05	1.3	−175	0.85	1.00	...
		3	0.06	3.8	−166	1.71	1.00	...
		4	0.09	9.6	−166	1.90	1.00	...
	2.3	1	0.44	0.0	...	1.48	1.00	...
		2	0.16	3.2	−168	2.10	1.00	...
		3	0.19	9.3	−164	2.49	1.00	...
	1.6	1	0.51	0.0	...	3.64	1.00	...
		2	0.27	7.9	−166	4.10	1.00	...
		3	0.01	25.1	−176	6.15	1.00	...
		4	0.01	38.7	−174	7.10	1.00	...
	0.61	1	0.85	0.0	...	11.98	0.71	59
	0.33	1	0.37	0.0	...	14.77	1.00	...

TABLE 3—*Continued*

Source	ν (GHz)	Comp. Number	S (Jy)	r (mas)	θ (deg)	a (mas)	b/a	ϕ (deg)
J1656+6012	8.4	1	0.20	0.0	...	0.48	0.50	−50
	2.3	1	0.19	0.0	...	1.14	1.00	...
	1.6	1	0.18	0.0	...	2.27	1.00	...
J1746+6226	15	1	0.43	0.0	...	0.24	1.00	...
	8.4	1	0.61	0.0	...	0.32	0.48	46
		2	0.01	2.0	−144	1.24	1.00	...
	2.3	1	0.22	0.0	...	0.89	0.27	38
		2	0.03	2.3	−144	0.72	1.00	...
		3	0.01	5.5	−151	2.80	1.00	...
		4	0.03	14.8	−150	3.26	1.00	...
		5	0.02	24.3	−148	5.15	1.00	...
		6	0.02	44.4	−150	19.53	1.00	...
	1.6	1	0.21	0.0	...	2.57	1.00	...
		2	0.05	14.0	−150	4.89	1.00	...
		3	0.03	23.1	−150	5.01	1.00	...
		4	0.02	34.0	−148	9.62	1.00	...
J1812+5603	8.4	1	0.22	0.0	...	0.33	1.00	...
	2.3	1	0.26	0.0	...	0.97	1.00	...
	1.6	1	0.22	0.0	...	1.04	1.00	...
		2	0.01	7.3	113	1.65	1.00	...
J1823+6857	8.4	1	0.46	0.0	...	0.13	1.00	...
		2	0.19	0.3	−20	0.69	1.00	...
	2.3	1	0.60	0.0	...	0.70	1.00	...
		2	0.03	2.6	24	5.32	1.00	...
	1.6	1	0.55	0.0	...	1.28	1.00	...
	0.33	1	0.22	0.0	...	20.59	1.00	...
J1927+6117	8.4	1	0.85	0.0	...	0.41	0.25	−45
		2	0.56	0.9	117	0.34	1.00	...
	2.3	1	1.43	0.0	...	1.07	0.41	−36
		2	0.05	4.1	180	7.78	1.00	...
	1.6	1	1.15	0.0	...	1.11	1.00	...
		2	0.15	2.4	130	1.70	1.00	...
J2002+4725	8.4	1	0.60	0.0	...	0.28	1.00	...
	2.3	1	0.71	0.0	...	1.12	1.00	...
	1.6	1	0.58	0.0	...	1.43	1.00	...
		2	0.05	2.4	49	2.03	1.00	...
J2009+7229	1.6	1	1.07	0.0	...	0.51	1.00	...
		2	0.18	1.2	−126	5.29	1.00	...
		3	0.04	16.2	−154	12.55	1.00	...
	0.61	1	0.91	0.0	...	8.75	0.63	−74
	0.33	1	0.23	0.0	...	13.44	1.00	...
J2022+6136	8.4	1	1.46	0.0	...	0.33	1.00	...
		2	0.65	0.4	40	0.68	1.00	...
		3	0.14	2.5	35	1.48	1.00	...
		4	0.72	7.0	33	0.51	1.00	...
		5	0.13	7.6	34	0.61	1.00	...
		6	0.04	9.7	41	0.77	1.00	...
	2.3	1	1.48	0.0	...	2.70	1.00	...
		2	1.25	6.6	−146	2.94	1.00	...
	1.6	1	1.08	0.0	...	3.36	1.00	...
		2	0.89	6.8	31	3.40	1.00	...
		3	0.08	8.7	118	2.94	1.00	...
	0.61	1	1.36	0.0	...	13.51	0.74	−39
	0.33	1	0.77	0.0	...	36.02	0.75	−26
J2230+6946	8.4	1	0.19	0.0	...	0.29	1.00	...
		2	0.05	1.0	73	0.63	1.00	...
	2.3	1	0.36	0.0	...	0.82	1.00	...
		2	0.08	1.9	40	1.05	1.00	...
		3	0.03	14.5	42	8.35	1.00	...
	1.6	1	0.22	0.0	...	1.33	1.00	...
		2	0.04	2.8	41	2.03	1.00	...
		3	0.02	13.3	42	4.57	1.00	...
		4	0.01	20.3	53	6.97	1.00	...
		5	0.01	42.8	72	22.05	1.00	...
	0.33	1	0.28	0.0	...	24.59	1.00	...

TABLE 3—*Continued*

Source	ν (GHz)	Comp. Number	S (Jy)	r (mas)	θ (deg)	a (mas)	b/a	ϕ (deg)
J2311+4543	8.4	1	0.45	0.0	...	0.65	0.24	−41
		2	0.02	2.0	118	1.72	1.00	...
	2.3	1	0.45	0.0	...	0.64	1.00	...
		2	0.05	2.4	113	2.17	1.00	...
		3	0.01	11.6	113	2.21	1.00	...
	1.6	1	0.39	0.0	...	0.80	1.00	...
		2	0.05	2.8	110	1.99	1.00	...
		3	0.01	13.5	114	6.53	1.00	...

NOTES.—The models fitted to the visibility data are of Gaussian form with flux density S and FWHM major axis a and minor axis b, with major axis in position angle ϕ (measured north through east). Components are separated from the (arbitrary) origin of the image by an amount r in position angle θ, which is the position angle (measured north through east) of a line joining the components with the origin. Table 3 is also available in machine-readable form in the electronic edition of the *Astrophysical Journal Supplement*.

fraction,'' which is the ratio of core flux density to total flux density defined as

$$\frac{\sum_i (S_i)_{\rm beam}}{\sum_i S_i}, \qquad (1)$$

where S_i is the flux density of the ith CLEAN component. Thus, core flux density is defined as the sum of the CLEANed flux density within one synthesized beam and the total flux density is defined as the total CLEANed flux density (i.e., the sum of all CLEAN components).

In order to make a direct comparision with the results of Ojha et al. (2004a) we calculate the core fraction only at 8.4 GHz. At 8.4 GHz there are 42 images equally divided between scintillators and nonscintillators. Although most of the nonscintillators (18/21) overlap with the sample of Ojha et al. (2004a), almost half the scintillators (9/21) are different, so it is worthwhile repeating this test here.

The scintillating (nonscintillating) sources have mean core fraction of 0.89 (0.66) with median value of 0.92 (0.62). A Kolmogorov-Smirnov (K-S) test (Press et al. 1992; Kolmogorov 1933; Smirnov 1936) reveals that there is over 99% chance that both these samples are derived from different core fraction populations. Thus, the present observations further confirm the results of Ojha et al. (2004a) that scintillators are significantly more core dominated than nonscintillators. More comprehensive analysis, including an assessment of the role of scattering in explaining this difference, is the subject of future work.

4. SUMMARY

We have presented milliarcsecond scale images at up to seven frequencies for 49 scintillating and nonscintillating extragalactic radio sources selected from the MASIV survey. These data, assembled from our own observations and existing observations from the RRFID, provide a large sample for the study of angular broadening in both types of sources. They also expand the available milliarcsecond scale morphological information on scintillating and nonscintillating sources. A companion paper uses these observations to assess the impact of scattering on these sources.

This research has made use of the United States Naval Observatory (USNO) Radio Reference Frame Image Database (RRFID). Basic research in radio astronomy at the NRL is supported by the Office of Naval Research. This research has made use of NASA's Astrophysics Data System Bibliographic Services. R. Ojha dedicates this paper to the memory of Bateshwar Ojha.

REFERENCES

Bignall, H. E. 2003, Ph.D. thesis, Univ. Adelaide
Bignall, H. E., Macquart, J.-P., Jauncey, D. L., Lovell, J. E. J., Tzioumis, A. K., & Kedziora-Chudczer, L. 2006, ApJ, in press
Bignall, H. E., et al. 2003, ApJ, 585, 653
———. 2004, in Proc. 7th European VLBI Network Symp., ed. R. Bachiller, F. Colmer, J. F. Desmurs, & P. de Vicente (Toledo: Obs. Astron. Nacional de Spain), 19
Bridle, A. H., & Greisen, E. W. 1994, AIPS Memo. 87
Dennett-Thorpe, J., de Bruyn, A. G. 2002, Nature, 415, 57
———. 2003, A&A, 404, 113
Fey, A. L., & Charlot, P. 2000, ApJS, 128, 17
Greisen, E. W. 1988, AIPS Memo. 61
Jauncey, D. L., Bignall, H. E., Lovell, J. E. J., Kedziora-Chudczer, L., Tzioumis, A. K., Macquart, J.-P., & Rickett, B. J. 2000, in Astrophysical Phenomena Revealed by Space VLBI, ed. H. Hirabayashi, P. G. Edwards, & D. W. Murphy (Sagamihara: ISAS), 147
Jauncey, D. L., Johnston, H. M., Bignall, H. E., Lovell, J. E. J., Kedziora-Chudczer, L., Tzioumis, A. K., & Macquart, J.-P. 2003, Ap&SS, 288, 63
Jauncey, D. L., Lovell, J. E. J., Koyama, Y., & Kondo, T. 2005, AJ, submitted
Jauncey, D. L., & Macquart, J.-P. 2001, A&A, 370, L9
Kolmogorov, A. 1933, G. Ist. Attuari, 4, 83
Lazio, T. J. W., Cordes, J. M., & Fey, A. L. 2005, Science, submitted
Lovell, J. E. J., Jauncey, D. L., Bignall, H. E., Kedziora-Chudczer, L., Macquart, J.-P., Rickett, B. J., & Tzioumis, A. K. 2003, AJ, 126, 1699
Macquart, J.-P., & Jauncey, D. L. 2002, ApJ, 572, 786
Ojha, R., Fey, A., Jauncey, D. L., Lovell, J. E. J., & Johnston, K. J. 2004a, ApJ, 614, 607
Ojha, R., Fey, A., Lovell, J. E. J., Jauncey, D. L. and Johnston, K. J. 2004b, AJ, 128, 1570
Press, W. H., Teukolsky, S. A., Vetterling, W. T., & Flannery, B. P. 1992, Numerical Recipes in C: The Art of Scientific Computing (Cambridge: Cambridge Univ. Press), 623
Quirrenbach, A., Witzel, A., Kirchbaum, T. P., Hummel, C. A., Wegner, R., Schalinski, C. J., Ott, M., Alberdi, A., & Rioja, M. 1992, A&A, 258, 279
Rickett, B. J. 1990, ARA&A, 28, 561
Rickett, B. J., Witzel, A., Kraus, A., Krichbaum, T. P., & Qian, S. J. 2001, ApJ, 550, L11
Shepherd, M. C. 1997, in ASP Conf. Ser. 125, Astronomical Data Analysis Software and Systems VI, ed. G. Hunt & H. E. Payne (San Francisco: ASP), 77
Smirnov, N. V. 1936, C. R. Acad. Sci. Paris, 202, 449
Taylor, G. B., Vermeulen, R. C., Readhead, A. C. S., Pearson, T. J., Henstock, D. R., & Wilkinson, P. N. 1996, ApJS, 107, 37
Walker, M. A. 1998, MNRAS, 294, 307